

# Study of Synchronisation in Chains of Coupled Non-linear Oscillators and Resonators

RITA GUPTA

MSc by Research in Pattern Analysis and Neural Networks



ASTON UNIVERSITY

September 2008

This copy of the thesis has been supplied on condition that anyone who consults it is understood to recognise that its copyright rests with its author and that no quotation from the thesis and no information derived from it may be published without proper acknowledgement.

# Acknowledgements

First and foremost, my thanks to Professor David Lowe, my supervisor, for his many comments, suggestions, and stimulating discussions, which helped drive the project to its present form.

I'd like to acknowledge the support of my fellow MSc students, especially, Ain, for her support and encouragement throughout the MSc programme.

My special thanks also go to Diar Nasiev, James and András Joó for their help on countless occasions, and, in general, to NCRG for its collegiate and friendly environment.

Last, but not the least, I thank my mum for always encouraging me to follow my dreams.

ASTON UNIVERSITY

# Study of Synchronisation in Chains of Coupled Non-linear Oscillators and Resonators

RITA GUPTA

MSc by Research in Pattern Analysis and Neural Networks, 2008

## Thesis Summary

The aim of this Research Project was to study synchronisation in one-dimensional chains of coupled nonlinear systems, such as van der Pol oscillator and Duffing resonator. The results were obtained using numerical experiments, and, where appropriate, are discussed in terms of the linear perturbation theory and the recently proposed Partial Contraction theory [1]. Simple nonlinear systems, such as Duffing resonator, provide a good understanding of the nonlinear properties of MEMS [2] [3] and NEMS [4] devices. Therefore, the results obtained here are also discussed in the context of application to MEMS and NEMS resonators and their arrays.

**Keywords:** MEMS, NEMS, van der Pol oscillator, Duffing resonator, synchronisation, contraction, partial contraction, phase portrait, limit cycle, hysteresis, Fermi Pasta Ulam chains, intrinsic local modes (ILMs)

# Contents

<b>1</b>	<b>Introduction</b>	<b>9</b>
1.1	Motivation for the Project . . . . .	9
1.2	MEMS: A Brief Overview . . . . .	10
1.2.1	MEMS as Duffing resonator . . . . .	11
1.3	Synchronisation and Networks . . . . .	13
1.4	Theoretical Considerations . . . . .	14
1.5	Plans for the Rest of the Thesis . . . . .	15
<b>2</b>	<b>Single and Two- Coupled Nonlinear Oscillators</b>	<b>16</b>
2.1	Single Nonlinear Oscillators . . . . .	16
2.1.1	van der Pol Oscillator . . . . .	16
2.1.2	Duffing Resonator . . . . .	18
2.1.3	Hysteresis in the Duffing Resonator . . . . .	21
2.2	Two Coupled Oscillators . . . . .	24
2.2.1	Coupled van der Pol Oscillators . . . . .	24
2.2.2	Coupled Duffing Resonators . . . . .	26
2.2.3	Coupled Duffing-van der Pol Oscillators . . . . .	29
2.3	Summary . . . . .	30
<b>3</b>	<b>Partial Contraction Theory</b>	<b>31</b>
3.1	Contraction and Partial Contraction . . . . .	31
3.2	Ring of Four Coupled Oscillators . . . . .	32
3.2.1	Oscillator Ring with Two-way Coupling . . . . .	32
3.2.2	Oscillator Ring with One-way Coupling . . . . .	34
3.3	Networks with General Structures . . . . .	36
3.4	Summary . . . . .	37
<b>4</b>	<b>Chain of Identical Oscillators</b>	<b>38</b>
4.1	Linear Oscillators: Fermi Pasta Ulam Model . . . . .	38
4.1.1	Fermi Pasta Ulam Paradox . . . . .	39
4.1.2	Discrete Breathers . . . . .	40
4.2	Dynamic Systems: Chain of van der Pol Oscillators . . . . .	41
4.2.1	Measures of Synchronisation . . . . .	41
4.2.2	Velocity Coupling . . . . .	42
4.2.3	Displacement Coupling . . . . .	45
4.3	Dynamic System with Added Nonlinear Spring Constant . . . . .	46
4.3.1	Velocity Coupling . . . . .	47

## CONTENTS

4.3.2	Displacement Coupling . . . . .	48
4.4	Effect of Frequency Distribution . . . . .	49
4.5	Comparison with Partial Contraction Theory . . . . .	50
4.6	Summary . . . . .	52
<b>5</b>	<b>Chains of Coupled Hybrid Oscillators</b>	<b>53</b>
5.1	Chain of Duffing Resonators . . . . .	53
5.2	Hybrid Duffing - van der Pol Systems . . . . .	56
5.2.1	Alternating Duffing - van der Pol Oscillators . . . . .	57
5.2.2	Duffing Chain Driven by van der Pol Oscillators . . . . .	60
5.3	Summary and Relevance to MEMS Arrays . . . . .	62
<b>6</b>	<b>Conclusions</b>	<b>64</b>
<b>A</b>	<b>Derivation of van der Pol Equation</b>	<b>67</b>
<b>B</b>	<b>A Damped van der Pol Oscillator: Contraction Properties</b>	<b>68</b>
<b>C</b>	<b>Linear Perturbation Theory for a Chain of Oscillators</b>	<b>69</b>

# List of Figures

1.1	Schematic diagram of actuators: (a) Parallel plate capacitor. and, (b) Comb drive capacitor. . . . .	11
1.2	Schematic diagram of a longitudinal mode beam resonator. . . . .	11
1.3	Electrical equivalent circuit for the longitudinal mode beam resonator. . . . .	12
1.4	Coupled two-, chain and globally connected network of oscillators . . . . .	13
2.1	Electric circuit corresponding to van der Pol oscillator. . . . .	17
2.2	Phase portrait of a van der Pol oscillator showing limit cycles for $\rho = 1$ , and, (a) $\mu = 0.5$ , (b) $\mu = 2.5$ . The limit cycle changes from circular to diamond shape as $\mu$ increases. . . . .	17
2.3	Phase portrait for a single (undamped, unforced) Duffing oscillator with $\alpha = 1, \beta = -1$ . . . . .	19
2.4	Phase portrait (a) and time trajectory (b) for a chaotic Duffing oscillator ( $\alpha = -1, \beta = 1, \delta = 0.1, \Gamma = 0.35$ and $\omega = 1.4$ ). . . . .	20
2.5	Phase portrait for a van der Pol- Duffing oscillator exhibiting limit cycle behaviour ( $\alpha = -1, \beta = 0.5$ and $\mu = 0.1$ ). . . . .	20
2.6	Duffing resonator showing hysteresis for (a) $\beta > 0$ ( $\alpha = \beta = 1, \delta = 0.1$ and $\Gamma = 1$ ), and (b) $\beta < 0$ ( $\alpha = 79.5, \beta = -13.25, \delta = 0.052$ and $\Gamma = 0.6$ ) [5]. . . . .	22
2.7	The Duffing resonator (a) showing jump phenomena (dashed lines) and hysteresis, and, (b) the transition (ring-down time) for the jump from upper to lower branch as the frequency is increased from $\omega = 12 \cdot 10^3 \text{Rad s}^{-1}$ to $\omega = 12.5 \cdot 10^3 \text{Rad s}^{-1}$ at $t=150$ ms. . . . .	23
2.8	Two identical $x$ -coupled van der Pol oscillators ( $\rho = 1, \mu = 2.5$ , and, $k = 0.7$ ) showing (a) anti-phase locking, and, (b) synchronisation for initial values of $\dot{x}_1[0] = \dot{x}_2[0] = 0, x_2[0] = 1.2$ , and, $x_1[0] = -0.1$ for (a) and $x_1[0] = 0.01$ for (b). . . . .	25
2.9	Two identical van der Pol oscillators coupled through the velocity term showing (a) synchronisation, and, (b) oscillator death. . . . .	26
2.10	Two non-identical velocity coupled van der Pol oscillators with $\kappa_1 + \kappa_2 > 1$ showing (a) synchronisation when $\rho_1 - \rho_2$ small ( $\rho_1 = 2.0, \rho_2 = 1.5, \mu_1 = \mu_2 = 1.7$ ), and, (b) non-synchronous behaviour when $\rho_1 - \rho_2$ large ( $\rho_1 = 2.9, \rho_2 = 1.8, \mu_1 = 0.83, \mu_2 = 1.7$ ). . . . .	27
2.11	Time trajectories of two identical diffusively $x$ - coupled Duffing resonators, where only one of them (shown in red) is driven externally. The values of parameters used is: $\alpha = \beta = \Gamma = 1, \delta = 0.1$ , and, the initial values are same for all four cases. . . . .	27

LIST OF FIGURES

2.12	Frequency-dependence of the amplitude of the master resonator (blue), and the ratio of the amplitudes of the slave to that of the master (magenta), for both $x$ - and velocity- coupling. The values of parameters used are: $\alpha = 100, \beta = 10, \Gamma = 5, \delta = 0.1$ , and, the initial values are same for all four cases. . . . .	28
2.13	$x$ -coupled (a) and velocity-coupled (b) van der Pol oscillator (red) and Duffing resonator (blue) for $\rho = \alpha = \beta = \mu = K = 1$ and $\delta = 0.2$ . . . . .	30
3.1	A ring of four oscillators with two-way coupling. . . . .	33
3.2	A ring of four oscillators with one-way coupling. . . . .	34
3.3	Time trajectories for a ring of four velocity-coupled van der Pol oscillators with (a) two-way coupling, and, (b) one-way coupling. . . . .	36
4.1	Displacement of simple oscillators in a chain with non-linear coupling index $\nu = 3$ , and coupling constant $\eta = 0.5$ : (a) at $t=6030$ , and (b) at $t=0$ and $t=6031$ . . . . .	39
4.2	Formation of discrete breathers in a chain of linear oscillators where $\nu = 3$ , and, the non-linear coupling strength $\eta = 0.05$ : (a) Initial displacement of the chain of oscillators in the $\beta$ mode, (b) odd- mode breather ( $t = 565$ ), (c) two coupled even- mode breathers ( $t = 810$ ), and, (d) an odd- mode breather surrounded by even- mode breathers ( $t = 650$ ). . . . .	40
4.3	(a) Time-dependence of the displacement of the 32 velocity-coupled van der Pol oscillators, and, (b) oscillator displacement along the chain for $t=0$ . . . . .	43
4.4	Time-dependence of the displacement of a chain of 32 velocity-coupled van der Pol oscillators showing emergence of cooperative behaviour: (a) time trajectories and (b) oscillator displacement along the chain for $t=200$ . . . . .	43
4.5	(a) Time-dependence of the displacement of the 32 velocity-coupled van der Pol oscillators, and (b) oscillator displacement along the chain for $t=99700$ . . . . .	44
4.6	Phase portrait of the 32 velocity-coupled van der Pol oscillators ( $\mu = \kappa = 0.01$ ). . . . .	44
4.7	Variation of $t_s$ , time needed to achieve 90% synchronisation ( $C_s = 0.9$ ), with the coupling constant $\kappa$ for various values of $\mu$ in velocity-coupled chains of van der Pol oscillators; $C_s$ was calculated using Equation (4.3). . . . .	45
4.8	(a) Time trajectories, and, (b) oscillator displacement for $x$ -coupled chain of van der Pol oscillators for $\mu = 0.1$ and total coupling $\mu\kappa = 2$ . . . . .	46
4.9	The measure of phase synchronisation ( $\mu = 0.1$ ), and, displacement synchronisation ( $\mu = 0.5, 1$ and $3$ ), plotted against the (total) coupling constant $\mu\kappa$ for a chain of $x$ - coupled van der Pol oscillators. . . . .	47
4.10	Time trajectories of velocity-coupled identical van der Pol - Duffing oscillators with $\mu = 0.1, \kappa = 4$ , (a) showing complete synchronisation for $\beta = 0.1$ and (b) incomplete synchronisation for $\beta = 0.25$ . . . . .	48

LIST OF FIGURES

4.11	Evolution of complete synchronisation for a chain of $x$ -coupled identical van der Pol - Duffing oscillators for $\mu = 1$ , $\beta = 0.1$ and coupling constant $k = 0.1$ . . . . .	48
4.12	Minimum coupling constant $k$ required for 90 % synchronisation ( $C_s = 0.9$ ) by $t=1000$ , vs $\beta$ , in chains of $x$ - coupled van der Pol - Duffing oscillators, for various values of $\mu$ , . . . . .	49
4.13	Time trajectories for $\mu = 0.1$ , relative coupling constant $\kappa(k) = 2$ and 20% frequency spread: (a) velocity-coupled van der Pol oscillators, and (b) $x$ -coupled van der Pol - Duffing oscillators with $\beta = 0.5$ . The velocity coupled chain of van der Pol - Duffing oscillators shows unsynchronised motion for these parameters. . . . .	50
4.14	Time trajectories for $\mu = 1$ , relative coupling constant $\kappa(k) = 0.5$ and 20% frequency spread: (a) velocity-coupled van der Pol oscillators, and (b) velocity-coupled van der Pol - Duffing oscillators with $\beta = 0.5$ . The $x$ - coupled chain of van der Pol - Duffing oscillators shows less synchronisation for these parameters. . . . .	50
5.1	The time trajectories (a), and, oscillator displacements along the chain (b), for a chain of $x$ - coupled Duffing resonators forced with frequency $\omega = 1.6$ from one end. . . . .	54
5.2	The time trajectories (a), and, oscillator displacements along the chain (b), for a chain of $x$ - coupled Duffing resonators forced with frequency $\omega = 1.6$ from the middle of the chain. . . . .	55
5.3	The oscillator displacements along the chain of Duffing resonators forced with frequency $\omega = 2.3$ , from one end of the chain (a), and, from the middle of the chain (b). . . . .	55
5.4	The time trajectories (a), and, oscillator displacements along the chain (b), for a velocity-coupled chain of Duffing resonators forced with frequency $\omega = 1.6$ from one end. . . . .	56
5.5	The time trajectories (a), and, oscillator displacements along the chain (b), for a velocity-coupled chain of Duffing resonators forced with frequency $\omega = 1.6$ from from the middle of the chain. . . . .	56
5.6	Time trajectories and displacement along the chain for (a) the van der Pol sublattice, and, (b) for the Duffing sublattice, for $\mu = 0.1$ . Both time trajectories and oscillator displacement show that the van der Pol sublattice is more entrained compared to the Duffing sublattice. . . . .	57
5.7	Time trajectories for (a) the van der Pol sublattice, and (b) for the Duffing sublattice, for $\mu = 1$ . . . . .	58
5.8	Phase portraits of velocity- coupled chain of alternating van der Pol and Duffing oscillators for $\mu = 1$ for van der Pol sublattice (blue) and for the Duffing sublattice (magenta). . . . .	58
5.9	Time trajectories for the van der Pol (a) and the Duffing (b) sublattices for $\mu = 1$ , showing time-delay synchronisation. . . . .	59
5.10	Instantaneous displacement along the chain for a velocity-coupled chain of alternating Duffing and van der Pol systems. The displacement pattern for the van der Pol and the Duffing sublattices is similar. . . . .	60

*LIST OF FIGURES*

5.11 Time trajectories (a), and displacement along the chain (b), for the chain of  $x$ - coupled Duffing resonators with van der Pol forcing at both ends. The chain of Duffing resonators forms two sublattices as shown by splitting the time trajectories : (c) from  $i = 2, 16$  and (d) from  $i = 17, 31$ . 61

5.12 Time trajectories (a), and displacement along the chain (b), for the chain of velocity- coupled Duffing resonators with van der Pol forcing at both ends ( $i = 1, 32$ ). The chain of Duffing resonators forms two sublattices as shown by splitting the time trajectories : (c) from  $i = 2, 16$  and (d) from  $i = 17, 31$ . . . . . 62

5.13 Displacement along the chain for the Duffing resonators with van der Pol forcing at one end only (a) for  $x$ - coupling, and (b) for velocity coupling. 63

# Chapter 1

## Introduction

The aim of this thesis is to study entrainment in chains of coupled van der Pol oscillators and Duffing resonators, with a view to applications for MEMS and NEMS devices. In this chapter we first present the motivation for the Project (next section), while, a brief overview of MEMS and their relationship to the nonlinear Duffing resonator is presented in Section 1.2. The phenomenon of synchronisation is discussed in Section 1.3, which also contains a brief discussion on network geometries to couple the nonlinear oscillators. Some theoretical considerations are presented in Section 1.4, and, the chapter ends with a brief layout of the rest of the thesis

### 1.1 Motivation for the Project

Historically, van der Pol oscillator has been associated with the triode valve [6], and both, van der Pol and Duffing equations have been used to study the behaviour of coupled electrical circuits [7]. The study will also have relevance to the field of MEMS and NEMS, as discussed below:

MEMS (MicroElectroMechanical Systems) and NEMS (Nano ElectroMechanical Systems) have played an important role in the technological advancement in many fields [8], and, have a wide range of applications in the field of sensors [9], life sciences, photonics and communications [8], to name a few. As technology progresses, the size of the MEMS devices will decrease, making it easier to drive them into the nonlinear regime. Therefore, a good understanding of their nonlinear properties is vital for the

design of future devices.

Many applications of MEMS and NEMS, such as, optical switches [10] and mechanical spectrum analysis of electrical waveforms [11], involve arrays of MEMS. A system of coupled MEMS resonators has also been considered pattern recognition and mechanical neurocomputing [12]. Also, with diminishing device size, it becomes more difficult to isolate individual components. Therefore, it is anticipated that an understanding of the collective behaviour of arrays of MEMS and NEMS could be an important step in the design of future devices.

In this thesis we present a study of synchronisation in a chain of coupled nonlinear oscillators, with a view to understanding the collective behaviour of a class of MEMS and NEMS, namely, MEMS and NEMS resonators.

## 1.2 MEMS: A Brief Overview

MEMS devices can respond to external stimuli, for example in sensing applications, and, then, in response to the stimuli, move (or actuate) the mechanical part of the device. Some everyday examples include accelerometers in car airbags, pressure sensors and ink jet printers. Thus, as the name suggests, there are two parts to MEMS devices: sensors or actuators (electrical) and beams, diaphragms or nozzles etc. (mechanical). There are two types of actuators commonly used [13]: (i) Parallel plate capacitors, and, (ii) Comb drive capacitors. These are shown in Figure 1.1 schematically. For the parallel plate capacitor, the electrostatic load (composed of a DC voltage and a much smaller AC voltage), the mechanical restoring force and the damping force together govern the dynamic behaviour of the system. The DC voltage produces an electrostatic force on the moving plate, thereby moving it to a new equilibrium position, and the AC voltage drives the plate about this newly established position. The ratio of the mechanical motion to the electrostatic force is known as *transduction factor*  $\epsilon$ .

Next, we consider a longitudinal mode beam resonator which is excited with a parallel plate capacitor, and, derive the nonlinear differential equation associated with the system.

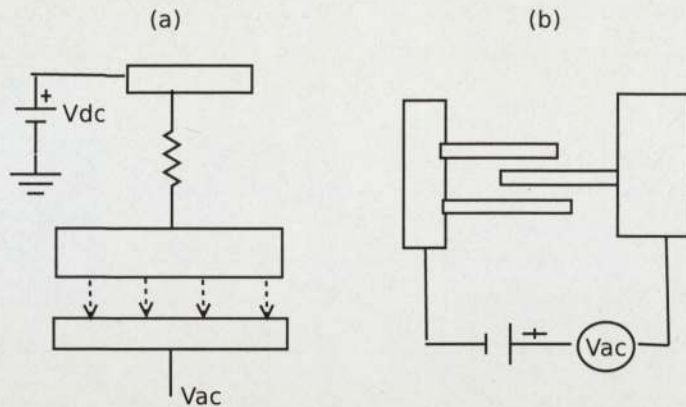


Figure 1.1: Schematic diagram of actuators: (a) Parallel plate capacitor. and, (b) Comb drive capacitor.

### 1.2.1 MEMS as Duffing resonator

Figure 1.2 shows a schematic diagram of a longitudinal mode beam resonator with half-length  $L$  and cross-sectional area  $A$ . The beam is fixed in the middle, is actuated symmetrically, and its ends move in opposite directions; The longitudinal displacement

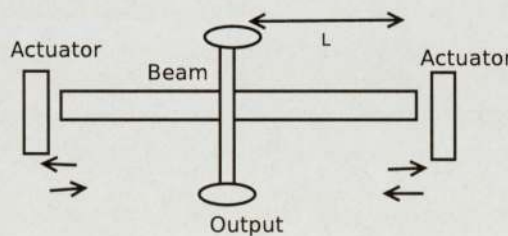


Figure 1.2: Schematic diagram of a longitudinal mode beam resonator.

of the beam,  $u$ , is governed by the wave equation [14]:

$$\rho A \frac{\partial^2 u}{\partial t^2} = \frac{\partial}{\partial z} \left( AY \frac{\partial u}{\partial z} \right), \quad (1.1)$$

where  $\rho$  is the beam density and  $Y$  is the nonlinear Young's modulus,

$$Y = \frac{T}{S} = Y_0(1 + Y_1 S + Y_2 S^2), \quad (1.2)$$

where  $T$  is force divided by area  $A$ ,  $S = \frac{\partial u}{\partial x}$  is the displacement gradient, and,  $Y_1$  and  $Y_2$  are the first order and second order corrections to the linear Young's modulus. If  $x$

CHAPTER 1. INTRODUCTION

represents the motion of the beam tip, solution to Equation (1.1) can be approximated as  $u(x, t) = x(t) \sin(\pi z/2L)$ . Thus, substituting for  $u(x, t)$  in Equation (1.1), we get

$$\rho AL \frac{\partial^2 u}{\partial t^2} = -\frac{\pi^2}{4} \frac{AY}{L} x \left( 1 + \frac{4Y_1}{3L} x + \frac{3\pi^2 Y_2}{16L^2} x^2 \right). \quad (1.3)$$

Equation (1.3) describes the nonlinear vibrations in a longitudinal mode beam resonator, and, can be rewritten as

$$m\ddot{x} + \gamma\dot{x} + k(x)x = F_\omega \cos(\omega t), \quad (1.4)$$

where,  $\gamma$  is the damping term,  $F_\omega$  is the forcing term at frequency  $\omega$ , and,

$$k(x) = k_0(1 + k_1x + k_2x^2), \quad (1.5)$$

with

$$m = \rho AL, \quad k_0 = \frac{\pi^2}{4} \frac{AY}{L}, \quad k_1 = \frac{4Y_1}{3L} \quad \text{and} \quad k_2 = \frac{3\pi^2 Y_2}{16L^2}. \quad (1.6)$$

Equation (1.4) is the ‘lumped model’ representation of the electromechanical resonator [14]. Figure 1.3 shows the electrical representation of the longitudinal mode beam

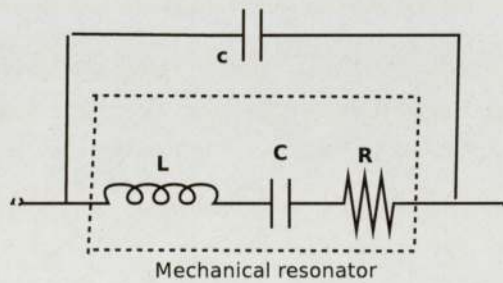


Figure 1.3: Electrical equivalent circuit for the longitudinal mode beam resonator.

resonator with capacitive excitation [15], where  $C = \varepsilon^2/k$ ,  $L = m/\varepsilon^2$ ,  $R = \sqrt{km}/(Q\varepsilon^2)$ , and, the quality factor  $Q = \sqrt{k/m}/(\gamma/m)$ .

In general,  $k_1$  is small, so that the electromechanical system can be represented by the Duffing equation

$$\ddot{x} + \delta\dot{x} + \alpha x + \beta x^3 = \Gamma \cos(\omega t), \quad (1.7)$$

with

$$\delta = \gamma/m, \quad \Gamma = F_\omega/m \quad \alpha = k_0/m \quad \text{and} \quad \beta = k_0k_2/m. \quad (1.8)$$

Thus, the quality factor  $Q$ , in terms of the parameters of the Duffing equation, is

$$Q = \sqrt{\alpha}/b. \tag{1.9}$$

The Duffing resonator of Equation(1.7) is discussed further in Subsection 2.1.2.

### 1.3 Synchronisation and Networks

Synchronisation is a cooperative behaviour of many-body interacting systems, where coordinated group behaviour is seen even though each individual acts independently. The Dutch researcher Christian Huygens was probably the first to discover the synchronisation phenomenon when he observed that two pendulum clocks, which were attached to a common beam, always moved in complete synchrony, but in opposite direction to each other [6]. Some of the examples of synchronisation from the natural world include bee swarms, bird flocking, schools of fish swimming together [16]; here, bees, birds, fish move with the same velocity through air/water, keeping a constant distance between them. The phenomenon is encountered in diverse fields such as physics, engineering, biology and social sciences. The study of cooperative phenomenon in coupled multiple systems has many applications: Recently, researchers working in the area of brain science have recognised the importance of rhythm and synchronisation of neurons in understanding brain function. [17], and those of cardiac cells in heart-beat [18]. Synchronisation in distributed multi agent system has also been simulated recently [19], and, the relevance of the phenomenon to MEMS and NEMS has already been discussed in Section 1.1.

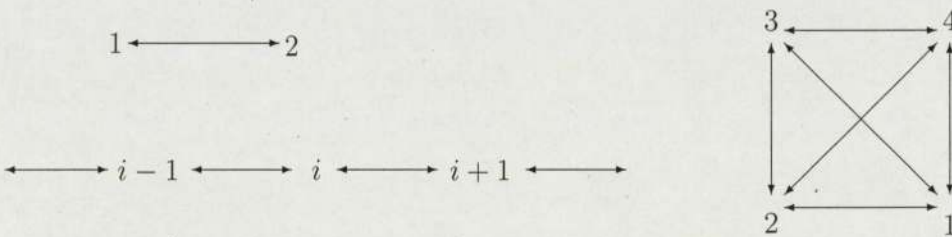


Figure 1.4: Coupled two-, chain and globally connected network of oscillators

## CHAPTER 1. INTRODUCTION

The process of synchronisation can be studied by modelling the behaviour of networks of coupled nonlinear oscillators. There can be many types of networks, ranging from simple geometries shown in Figure 1.4, to more complex networks such as scale-free and small world networks [20]. The coupling between any two oscillators can be linear [1] [21] [22], or, nonlinear [23]. A one-dimensional chain of oscillators is the simplest geometry of a network of coupled oscillators, where the interaction can be between the nearest neighbours, or with a group of neighbours [6]. A ring structure is encountered if the first and last members of the chain are coupled. A more interesting geometry is when all oscillators are globally connected to all other oscillators and the system goes through a transition (Kuramoto transition) where some of the oscillators synchronise spontaneously while others remain incoherent [6].

In this thesis, we consider synchronisation in two coupled oscillators (next chapter) and for chains of coupled oscillators (Chapters 4 and 5).

### 1.4 Theoretical Considerations

It is almost impossible to solve the second order differential equations describing the system of coupled nonlinear oscillators analytically, except for a few simple cases. In the literature, various perturbation methods have been used to solve these nonlinear differential equations [24], [25]. However, for more complex systems, such as networks of nonlinear oscillator, it becomes necessary to resort to finding numerical solutions.

However, there are some exceptions, such as Kuramoto model [17] discussed above, for which a general solution can be found. The recently proposed Partial Contraction Theory [1] has even wider application, where it extends the principle of contraction to obtain conditions for synchronisation for general networks of coupled nonlinear oscillators. So far, the theory has been applied to study the stability of synchronisation of identical oscillators only (van der Pol oscillators [1] and Lorenz [26] oscillators). A brief introduction to the theory will be presented in Chapter 3.

## 1.5 Plans for the Rest of the Thesis

A brief review of the properties of single van der Pol oscillator and Duffing resonator is presented in the next Chapter, and, some synchronisation properties of two- coupled systems explored. Chapter 3 presents a brief introduction to the Partial Contraction theory, while, Chapter 4 considers synchronisation in chains of identical unforced oscillators. Results of our numerical simulations for chains of Duffing resonators with external forcing, and, those for hybrid chains of Duffing resonator and van der Pol oscillator, are presented in Chapter 5. The main results of the thesis are summarised in Chapter 6.

## Chapter 2

# Single and Two- Coupled Nonlinear Oscillators

In this Chapter we review some of the key properties of the single van der Pol oscillator and the Duffing resonator which make them suitable for MEMS applications (Section 2.1). Also, the behaviour of a simple system of two-coupled nonlinear oscillators will be explored in Section 2.2.

### 2.1 Single Nonlinear Oscillators

#### 2.1.1 van der Pol Oscillator

The van der Pol oscillator was originally discovered by the Dutch physicist and engineer Balthasar van der Pol in 1927 when he found stable oscillations, known as limit cycles, in electrical circuits employing vacuum tubes. Driving these circuits near the limit cycle results in entrainment, i.e., the driving signal pulls the current along with it. van der Pol, together with his colleague van der Mark, were probably the first [27] to report deterministic chaos when they reported hearing irregular noise at certain driving frequencies [28].

The electric circuit with negative differential resistance, shown in Figure 2.1, can

be represented by the van der Pol equation [29],

$$\ddot{x} + \mu(x^2 - 1)\dot{x} + \rho x = 0, \quad (2.1)$$

where,  $\rho$  represents the strength of the harmonic part of the oscillator and  $\mu$  defines the strength of the nonlinear damping; the damping term is negative for small displacements ( $x(t) < 1$ ) and positive for large displacements ( $x(t) > 1$ ). The system decays to zero for  $\mu < 0$ . For  $\mu > 0$ , the nonlinearity term can be associated with negative resistance in a triode valve; This is shown in Appendix A. In this case, the

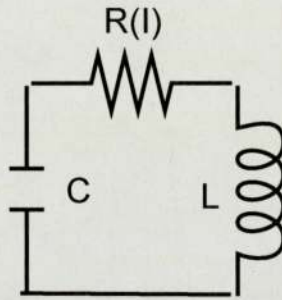


Figure 2.1: Electric circuit corresponding to van der Pol oscillator.

phase portrait of the oscillator is a limit cycle [25], i.e., all trajectories lead to the same cycle (Figure 2.2), with the exception of the case when  $x = \dot{x} = 0$ . The latter is an equilibrium point of the oscillator, obtained by setting  $\ddot{x} = 0$  and  $\dot{x} = 0$  in Equation (2.1).

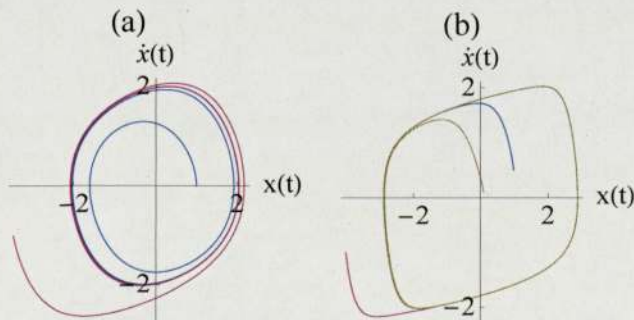


Figure 2.2: Phase portrait of a van der Pol oscillator showing limit cycles for  $\rho = 1$ , and, (a)  $\mu = 0.5$ , (b)  $\mu = 2.5$ . The limit cycle changes from circular to diamond shape as  $\mu$  increases.

Equation (2.1), which is a second order differential equation, can be linearised as:

$$\begin{aligned}\dot{x} &= y \\ \dot{y} &= -\mu(x^2 - 1)y - \rho x.\end{aligned}\tag{2.2}$$

Defining  $\dot{x} = f_1(x, y)$  and  $\dot{y} = f_2(x, y)$ , the Jacobian of the linearised system of equations is:

$$\mathbf{F} = \begin{pmatrix} \frac{\partial f_1}{\partial x} & \frac{\partial f_1}{\partial y} \\ \frac{\partial f_2}{\partial x} & \frac{\partial f_2}{\partial y} \end{pmatrix}\tag{2.3}$$

Linearisation of the second order differential equation, as shown in Equation (2.2), can be compactly written as

$$\dot{\mathbf{x}} = \mathbf{f}(\mathbf{x}, t),\tag{2.4}$$

where  $\mathbf{x} = (x, y)$  and  $\mathbf{f} = (f_1, f_2)$ , so that Equation (2.3) can be written as

$$\mathbf{F} = \frac{d\mathbf{f}}{d\mathbf{x}}.\tag{2.5}$$

The Jacobian matrix,  $F_{vdP}$  for Equations (2.2) is

$$\mathbf{F}_{vdP} = \begin{pmatrix} 0 & 1 \\ -\rho - 2\mu xy & -\mu(x^2 - 1) \end{pmatrix}\tag{2.6}$$

The real part of the eigenvalues, obtained on substituting  $x = \dot{x} = 0$  in Equation (2.6), is greater than zero; therefore, the equilibrium point  $(x, \dot{x})=(0,0)$  for Equation (2.1) is unstable, and is a repellant since all trajectories lead, even close to the equilibrium point, away from it (Figure 2.2 (b)). The limit cycle, on the other hand, is an attractor since trajectories with different initial values converge to the same cycle.

### 2.1.2 Duffing Resonator

For the van der Pol oscillator, the nonlinearity is in the velocity term  $\dot{x}$ ; The Duffing resonator, on the other hand, is nonlinear in the spring constant-term [30], and, as we saw in Subsection 1.2.1, it provides a framework for analysing the nonlinearities present in MEMS [2] [3] and NEMS [4]. The equation describing a damped, forced

Duffing resonator is

$$\ddot{x} + \delta\dot{x} + \alpha x + \beta x^3 = \Gamma \cos(\omega t), \quad (2.7)$$

where,  $\delta (> 0)$  and  $\Gamma$  are strengths of damping and the external driving force, respectively, and  $\omega$  is the frequency of the driving force. Both, linear and nonlinear spring constants,  $\alpha$  and  $\beta$ , respectively, can be positive or negative;  $\beta > 0$  represents a hard spring, whereas,  $\beta < 0$  represents a soft spring.

The phase portrait of the resonator for  $\alpha, \beta > 0$  are closed curves but not limit cycles, since they depend on the initial values of  $x$  and  $\dot{x}$ . There is only one equilibrium point at  $(x, \dot{x}) = (0, 0)$  which is stable for  $\delta > 0$ . For  $\alpha$  and  $\beta$  having opposite signs, the Duffing resonator can be expressed as motion in a double potential well ( $\alpha < 0, \beta > 0$ ), or in a double-hump potential ( $\alpha > 0, \beta < 0$ ) [30]. For this case, the resonator has two additional equilibrium points at  $(x, \dot{x}) = (\pm\sqrt{\alpha/\beta}, 0)$ . These points too are stable for  $\alpha, \delta > 0$ . As shown in Figure 2.3, the phase portrait for this case constitutes both closed and open curves, depending on the initial values of  $x$  and  $\dot{x}$  [21]. For some

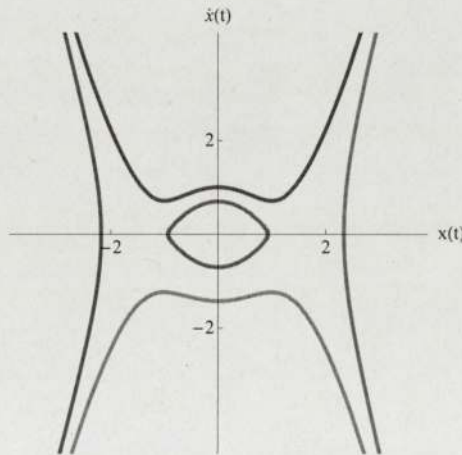


Figure 2.3: Phase portrait for a single (undamped, unforced) Duffing oscillator with  $\alpha = 1, \beta = -1$ .

parameters, the Duffing resonator can exhibit chaotic behaviour where, as shown in Figure 2.4, there is no sign of the resonator settling down to a periodic motion. The Duffing resonator also exhibits hysteresis behaviour in its frequency response, which has an important parallel in frequency-amplitude response in some MEMS [2] [3] and

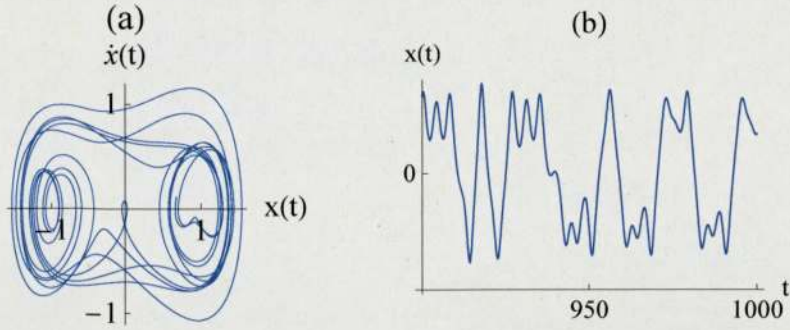


Figure 2.4: Phase portrait (a) and time trajectory (b) for a chaotic Duffing oscillator ( $\alpha = -1, \beta = 1, \delta = 0.1, \Gamma = 0.35$  and  $\omega = 1.4$ ).

NEMS [4] devices, and will be discussed in greater detail in Subsection 2.1.3.

Sometimes, the nonlinearities in spring constant and damping are combined in a single oscillator, viz.

$$\ddot{x} + \mu(x^2 - 1)\dot{x} + \alpha x + \beta x^3 = 0, \quad (2.8)$$

which has features of both van der Pol and Duffing oscillators. This is known as the van der Pol-Duffing oscillator [22] and exhibits limit cycle behaviour. This is shown in Figure 2.5.

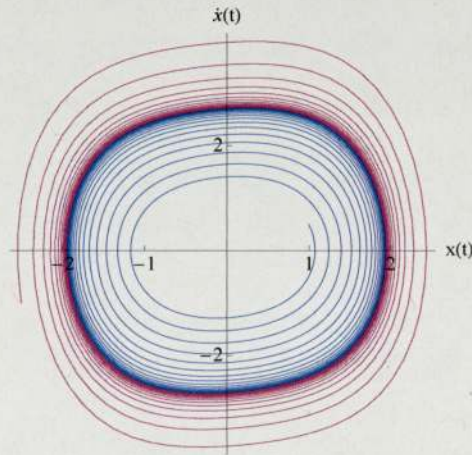


Figure 2.5: Phase portrait for a van der Pol- Duffing oscillator exhibiting limit cycle behaviour ( $\alpha = -1, \beta = 0.5$  and  $\mu = 0.1$ ).

The equilibrium points for this oscillator are similar to those for the Duffing res-

onator; Linearising Equation (2.8), one can write the Jacobian of the system as

$$\mathbf{F}_{\text{vdP-Duff}} = \begin{pmatrix} 0 & 1 \\ -\alpha - 3\beta x^2 - 2\mu xy & -\mu(x^2 - 1) \end{pmatrix}. \quad (2.9)$$

For the equilibrium point  $(x, \dot{x}) = (0, 0)$ , Equation (2.9) simplifies to

$$\mathbf{F}_{\text{vdP-Duff}}^0 = \begin{pmatrix} 0 & 1 \\ -\alpha & \mu \end{pmatrix} \quad (2.10)$$

which is similar to the Jacobian obtained for a van der Pol oscillator at its equilibrium point.

### 2.1.3 Hysteresis in the Duffing Resonator

In order to study the behaviour of a Duffing resonator around resonance, we assume that  $\beta \ll 1$  and  $\omega \approx \alpha$ , so that to first approximation

$$x(t) = A \cos(\omega t + \phi), \quad (2.11)$$

where  $\phi$  is a phase constant to be determined. Substituting Equation (2.11) in Equation (2.7), equating terms with  $\cos(\omega t)$  and  $\sin(\omega t)$ , and, neglecting higher harmonic terms, we get

$$[(\alpha - \omega^2)A + \frac{3}{4}\beta A^3] \cos \phi - \omega \delta A \sin \phi = \Gamma, \quad (2.12)$$

$$[(\alpha - \omega^2)A + \frac{3}{4}\beta A^3] \sin \phi + \omega \delta A \cos \phi = 0 \quad (2.13)$$

Multiplying Equation (2.12) with  $\cos \phi$  and Equation (2.13) with  $\sin \phi$ , and, adding the result we get

$$[(\alpha - \omega^2)A + \beta A^3] = \Gamma \cos \phi; \quad (2.14)$$

Similarly, multiplying Equation 2.12 with  $\sin \phi$  and Equation (2.13) with  $\cos \phi$ , and, subtracting the result from each other, we get

$$-\omega \delta A = \Gamma \sin \phi. \quad (2.15)$$

Finally, squaring Equations (2.14) and (2.15), and adding them together, we get

$$\left[ (\alpha - \omega^2)A + \frac{3}{4}\beta A^3 \right]^2 + (\delta A \omega)^2 = \Gamma^2. \quad (2.16)$$

Equation (2.16) describes the behaviour of the Duffing resonator near resonance, which is different from that of a linear oscillator, and, also, the behaviour is different for  $\beta > 0$  and  $\beta < 0$ ; This is shown in Figure 2.6, where the resonance peak bends

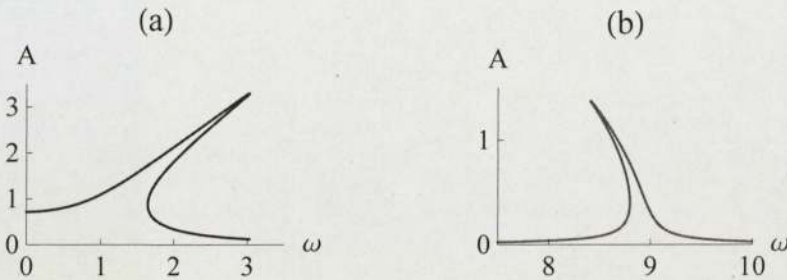


Figure 2.6: Duffing resonator showing hysteresis for (a)  $\beta > 0$  ( $\alpha = \beta = 1, \delta = 0.1$  and  $\Gamma = 1$ ), and (b)  $\beta < 0$  ( $\alpha = 79.5, \beta = -13.25, \delta = 0.052$  and  $\Gamma = 0.6$ ) [5].

to the right for the case of hard spring ( $\beta > 0$ ) (a) and to the left for the soft spring ( $\beta < 0$ ) (b). (The resonance peak of a linear oscillator does not bend.) The parameters,  $\alpha = \beta = 1, \delta = 0.1$  and  $\Gamma = 1$ , used for generating Figure 2.6 (a) were chosen randomly, and, will be used throughout the thesis for comparison purposes; This will be referred to as Duffing A. Parameters from a power systems device [5] were used for generating Figure 2.6 (b).

Figure 2.7 (a) shows the amplitude-frequency response for a Duffing resonator with  $\alpha = 100, \beta = 10, \delta = 0.1$  and  $\Gamma = 5$ ; These parameters are for a device built to sense small changes in mass [31], and will be referred to as Duffing B. The hysteresis curve was obtained numerically, i.e., without the approximations used for deriving Equation (2.16). From the Figure one can see that the amplitude of the Duffing resonator would follow different paths for increasing and decreasing frequencies: As the driving frequency increases from below the resonance (blue), the amplitude of the resonator increases up to the top of the curve; any further increase in the driving frequency results in a drop in the resonator amplitude, where it follows the lower branch of the  $A - \omega$  plot; This is known as the ‘Jump phenomena’ [30]. Starting from the high-frequency end (magenta), the amplitude increases gradually as the frequency increases, followed by a smaller jump, and merges with the upper curve. In Figure 2.7 (b) we plot the

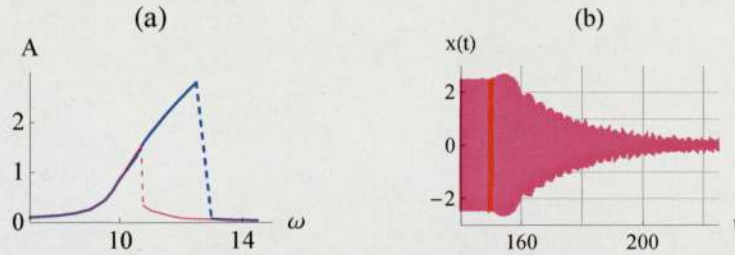


Figure 2.7: The Duffing resonator (a) showing jump phenomena (dashed lines) and hysteresis, and, (b) the transition (ring-down time) for the jump from upper to lower branch as the frequency is increased from  $\omega = 12. \cdot 10^3 \text{ Rad s}^{-1}$  to  $\omega = 12.5 \cdot 10^3 \text{ Rad s}^{-1}$  at  $t=150$  ms.

time trajectory of the Duffing resonator close to the high frequency jump,  $\omega \approx 12.0$ , where the effect of a slight increase in the frequency at  $t=150$  ms is also shown. As the frequency increases beyond the tip of the curve, the amplitude drops from  $A \approx 2$  to  $A \approx 0.2$  as expected; however there is a delay in the onset of the amplitude decrease, and, the amplitude is seen to decay to the new value instead of a sudden amplitude drop. This is known as the ‘Ring-down time’ [32], and, has been studied in greater detail by Zhang et al. [33]. Ring-down behaviour has been observed by Deng and Collins [31]; however, the delay in onset of ring-down observed by them is larger than that predicted by the theory.

In addition to the application of the hysteresis and jump phenomena associated with the Duffing resonator (Figure 2.7 (a)) for sensing changes in mass [32] [34], there are many other MEMS applications such as switches [35] and signal amplification [36] [37]. The quality factor  $Q$  (Equation (1.9)) is one of the most important characteristics of the MEMS resonators to be considered, especially for sensor application: higher the  $Q$ -value of the sensor, the better its performance. Grasser et al. [38] have proposed an artificial enhancement of the MEMS’  $Q$ -factor by modulating its stiffness at a harmonic frequency of the resonant frequency

## 2.2 Two Coupled Oscillators

In Section 2.1, we discussed some properties of the single van der Pol oscillator and the Duffing resonator; In the present Section, we explore the system when two of these oscillators are coupled to each other. In general the coupling can be diffusive or non-diffusive [23], linear or non-linear, mechanical [39] or reactive [40], and, may involve the displacement ( $x$ ), velocity ( $\dot{x}$ ), or a combination of the two. In this thesis we shall explore the effect of linear diffusive displacement and velocity couplings.

### 2.2.1 Coupled van der Pol Oscillators

Storti et al. [41] have considered the case of two identical van der Pol oscillators coupled through a combination of a linear diffusive displacement ( $x$ ) and velocity ( $\dot{x}$ ) coupling:

$$\begin{aligned}\ddot{x}_1 + \mu(x_1^2 - 1)\dot{x}_1 + \rho x_1 &= \mu k(x_2 - x_1) + \mu \kappa(\dot{x}_2 - \dot{x}_1), \\ \ddot{x}_2 + \mu(x_2^2 - 1)\dot{x}_2 + \rho x_2 &= \mu k(x_1 - x_2) + \mu \kappa(\dot{x}_1 - \dot{x}_2),\end{aligned}\tag{2.17}$$

where  $k$  and  $\kappa$  are the strengths for the two couplings, respectively. Four types of motions for the oscillators can be obtained depending on the initial values: the two oscillators can be in total in-phase synchrony, anti-phase locked, or slightly in phase or slightly anti-phase [41]. With only  $x$ - coupling present, the two oscillators can be synchronised in-phase or in anti-phase, depending on oscillator parameters and initial values [42]. This is shown in Figure 2.8 for  $\rho_1 = \rho_2 = 1$ ,  $\mu_1 = \mu_2 = 2.5$ , and,  $k_1 = k_2 = 0.7$ ; No such initial-value dependence is seen when the two oscillators are coupled through the velocity term only; this case is discussed next.

#### Velocity Coupling

In this Section we present a linear perturbation analysis to indicate transition in the system. We consider the general case of non-identical van der Pol oscillators with asymmetric velocity coupling:

$$\begin{aligned}\ddot{x}_1 + \mu_1(x_1^2 - 1)\dot{x}_1 + \rho_1 x_1 &= \mu_1 \kappa_1(\dot{x}_2 - \dot{x}_1), \\ \ddot{x}_2 + \mu_2(x_2^2 - 1)\dot{x}_2 + \rho_2 x_2 &= \mu_2 \kappa_2(\dot{x}_1 - \dot{x}_2).\end{aligned}\tag{2.18}$$

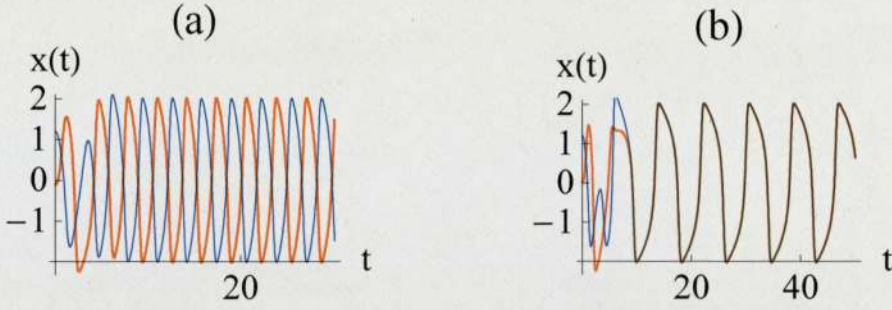


Figure 2.8: Two identical  $x$ -coupled van der Pol oscillators ( $\rho = 1$ ,  $\mu = 2.5$ , and,  $k = 0.7$ ) showing (a) anti-phase locking, and, (b) synchronisation for initial values of  $\dot{x}_1[0] = \dot{x}_2[0] = 0$ ,  $x_2[0] = 1.2$ , and,  $x_1[0] = -0.1$  for (a) and  $x_1[0] = 0.01$  for (b).

One of the equilibrium point for this system is  $(x_1, \dot{x}_1, x_2, \dot{x}_2) = (0, 0, 0, 0)$ . The two equations can be linearised as:

$$\begin{aligned} \dot{x}_1 &= y_1, & \dot{y}_1 &= -\mu_1(x_1^2 - 1)y_1 - \rho_1 x_1 + \mu_1 \kappa_1 (\dot{x}_2 - \dot{x}_1), \\ \dot{x}_2 &= y_2, & \dot{y}_2 &= -\mu_2(x_2^2 - 1)y_2 - \rho_2 x_2 + \mu_2 \kappa_2 (a\dot{x}_1 - \dot{x}_2), \end{aligned} \quad (2.19)$$

Similar to the case for a single oscillator (Subsection 2.1.1), the above equations can be compactly written as  $\dot{\mathbf{x}} = \mathbf{f}(\mathbf{x}, t)$ , where  $\mathbf{x} = (x_1, y_1, x_2, y_2)$ , and the Jacobian of the system is :

$$\mathbf{F} = \frac{d\mathbf{f}}{d\mathbf{x}}. \quad (2.20)$$

The system is said to be contracting, (i.e., all trajectories tend to a single trajectory asymptotically), if all eigenvalues  $\lambda_i$  of the Jacobian  $\mathbf{F}$  are negative, or, alternatively, if  $\mathbf{F}$  is negative definite [43].

Therefore, the Jacobian for identical oscillators, Equation (2.19) with  $\rho_1 = \rho_2$  and  $\mu_1 = \mu_2$ , at the equilibrium point  $(x_1, \dot{x}_1, x_2, \dot{x}_2) = (0, 0, 0, 0)$  is

$$F_{2vdP} = \begin{vmatrix} 0 & 1 & 0 & 0 \\ -\rho & -\mu(\kappa_1 - 1) & 0 & \mu\kappa_1 \\ 0 & 0 & 0 & 1 \\ 0 & \mu\kappa_2 & -\rho & -\mu(\kappa_2 - 1) \end{vmatrix},$$

with the characteristic equation

$$(\lambda^2 + \mu(\kappa_1 + \kappa_2 - 1))\lambda + \rho)(\lambda^2 - \mu\lambda + \rho) = 0. \quad (2.21)$$

From the above equation,  $\mathbf{F}$  has at least two positive roots for  $\mu > 0$ ; some roots of  $\mathbf{F}$  can be negative, and  $\mathbf{F}$  semi-negative definite, if  $\kappa_1 + \kappa_2 > 1$ . For this case, the system is contracting,  $\mathbf{x}_1 \rightarrow \mathbf{x}_2$  asymptotically and complete synchronisation will be achieved. Synchronisation of two identical oscillators is shown in Figure 2.9(a). The two identical oscillators can also be coupled in a way leading to oscillator death as shown in Figure 2.9(b) [1].

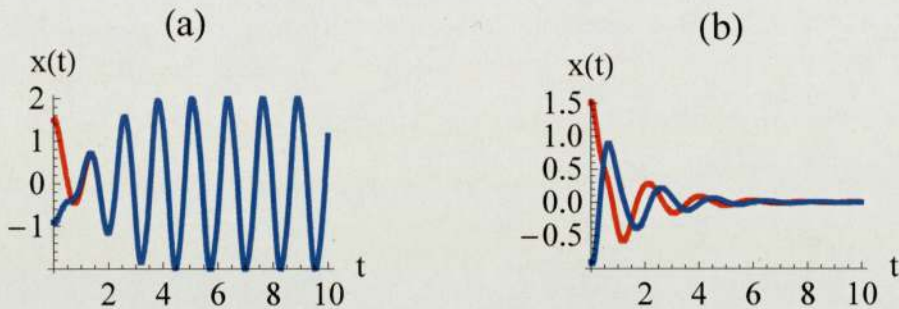


Figure 2.9: Two identical van der Pol oscillators coupled through the velocity term showing (a) synchronisation, and, (b) oscillator death.

For the case when the two velocity-coupled van der Pol oscillators are non-identical, the same condition,  $\kappa_1 + \kappa_2 > 1$  leads to synchronisation when  $\rho_1 - \rho_2$  is small, but the oscillators are not synchronised for large  $\rho_1 - \rho_2$ . This is shown in Figure 2.10. Therefore, the synchronicity of the coupled van der Pol oscillators depends on the off-diagonal terms of the Jacobian  $F_{2vdP}$ , whereas, from Equation (2.21), it is seen that the negative definite nature of the Jacobian depends only on its diagonal terms. This will be discussed further in Subsection 4.5.

## 2.2.2 Coupled Duffing Resonators

Fang et al. [44] and Raj et al. [23] have considered chaos and synchronisation in two coupled Duffing resonators with nonlinear  $x_i x_j^2$  coupling where both resonators were driven identically; the resonator trajectories were seen to be very sensitive to initial values of  $x$  and  $\dot{x}$  so that for some resonator parameters there can be as many as six attractors [23].

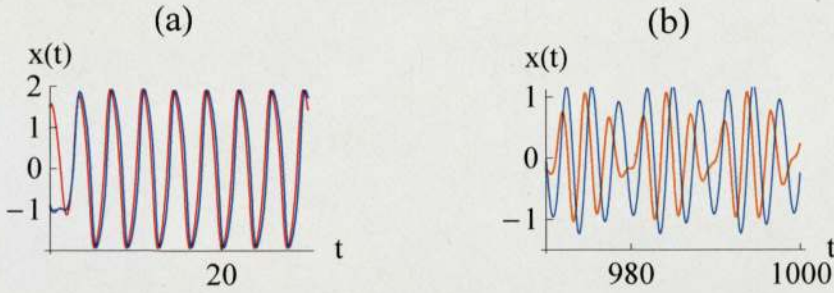


Figure 2.10: Two non-identical velocity coupled van der Pol oscillators with  $\kappa_1 + \kappa_2 > 1$  showing (a) synchronisation when  $\rho_1 - \rho_2$  small ( $\rho_1 = 2.0, \rho_2 = 1.5, \mu_1 = \mu_2 = 1.7$ ), and, (b) non-synchronous behaviour when  $\rho_1 - \rho_2$  large ( $\rho_1 = 2.9, \rho_2 = 1.8, \mu_1 = 0.83, \mu_2 = 1.7$ ).

Here we present time trajectories of two diffusively  $x$ -coupled identical Duffing resonators for  $\alpha = \beta = \Gamma = 1$  and  $\delta = 0.1$  (Duffing A), where only one resonator is driven externally. Velocity coupling leads to synchronisation of the two resonators, with the amplitude of the master resonator larger than that of the slave resonator (similar to Figure 2.11 (a)). Diffusive  $x$ - coupling, on the other hand, results in a more interesting behaviour, as shown in Figure 2.11 (a) - (d):

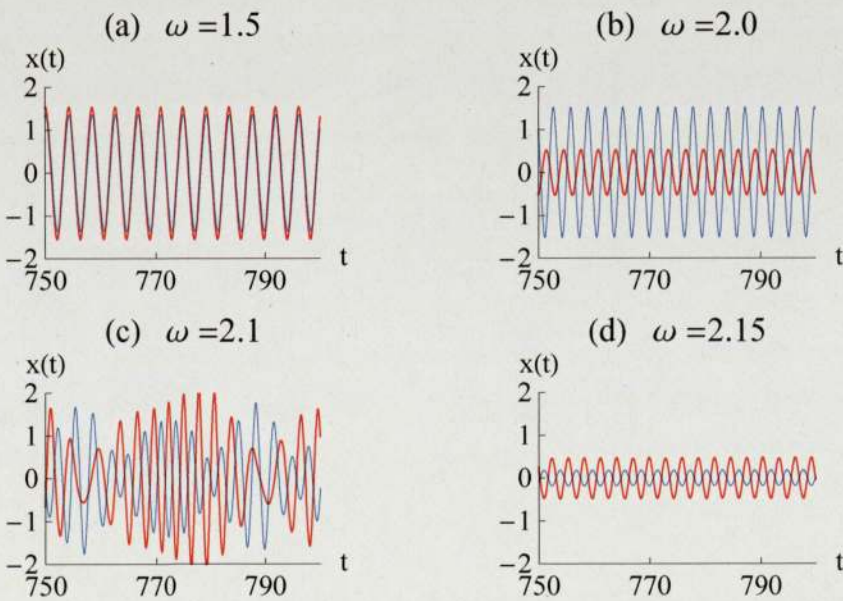


Figure 2.11: Time trajectories of two identical diffusively  $x$ - coupled Duffing resonators, where only one of them (shown in red) is driven externally. The values of parameters used is:  $\alpha = \beta = \Gamma = 1, \delta = 0.1$ , and, the initial values are same for all four cases.

For a range of frequencies, the two resonators are in phase with each other with almost equal amplitudes (Figure 2.11 (a)). Increasing the driving frequency, for another range of frequencies, the amplitude of the slave resonator (shown in blue) is larger than that of the master resonator (shown in red) (Figure 2.11 (b)); This is followed by non-synchronous chaotic behaviour exhibited by the resonators at  $\omega = 2.1$  (Figure 2.11 (c)), and a slight increase in the driving frequency results in a sudden decrease in amplitude for both resonators which are anti-phase locked (Figure 2.11 (d)). This jump-frequency is smaller than the corresponding frequency of  $\omega \approx 3$  for the single Duffing resonator (Figure 2.6 (a)) since the initial values of  $x$  and  $\dot{x}$  have been kept fixed for these calculations.

We have also considered two coupled Duffing resonators for the Duffing B system; Figure 2.12 shows the variation of the amplitude of the master resonator,  $A_1$ , and, the ratio of the amplitudes of the slave to that of the master,  $f$ , for both  $x$ - and velocity- coupling: The master resonator exhibits the usual jump phenomena, similar

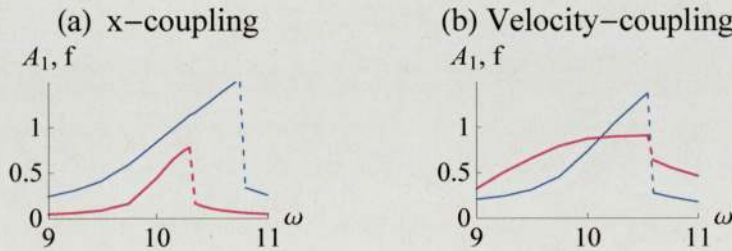


Figure 2.12: Frequency-dependence of the amplitude of the master resonator (blue), and the ratio of the amplitudes of the slave to that of the master (magenta), for both  $x$ - and velocity- coupling. The values of parameters used are:  $\alpha = 100, \beta = 10, \Gamma = 5, \delta = 0.1$ , and, the initial values are same for all four cases.

to that shown by a single Duffing resonator, (Figure 2.7 (a)). The slave resonator, on the other hand, while showing a smaller jump phenomena, shows different frequency responses for  $x$ - and velocity-couplings: For  $x$ -coupling the resonator has non-negligible amplitude only for a very small range of frequencies, while the velocity-coupling appears to be more effective in driving the slave resonator. The chaotic behaviour, and slave amplitude exceeding master amplitude, seen for coupled Duffing A, are not observed

for the coupled-Duffing B system.

### 2.2.3 Coupled Duffing-van der Pol Oscillators

Displacement coupling of two van der Pol - Duffing oscillator has been considered by Kadji and Yamapi [22] and by Criminale et al [21]; the former consider one-way diffusive  $K(x_1 - x_2)$  coupling of identical van der Pol-Duffing oscillators, described by Equation (2.8), while Criminale et al. consider non-diffusive  $x$ -coupling of (dissimilar) van der Pol oscillator and Duffing) resonators with  $\alpha < 0$  (the double-well Duffing). In this thesis, we consider the single-well Duffing resonators, corresponding to  $\alpha > 0$ , only.

We first consider a van der Pol oscillator coupled to a Duffing resonator with displacement- ( $u(x) = x$ ) or velocity- ( $u(x) = \dot{x}$ ) coupling:

$$\begin{aligned} \ddot{x}_1 + \mu(x_1^2 - 1)\dot{x}_1 + \rho x_1 &= K(u(x_2) - u(x_1)), \\ \ddot{x}_2 + \delta \dot{x}_2 + \alpha x_2 + \beta x_2^3 &= K(u(x_1) - u(x_2)). \end{aligned} \quad (2.22)$$

In the absence of any coupling, the amplitude of the Duffing resonator decays to zero while the van der Pol oscillator exhibits self-sustained oscillations. However, even a small coupling between the driving van der Pol oscillator and the Duffing resonator results in sustained oscillations by the Duffing resonator, the amplitude of oscillations increasing with the coupling constant. Figure 2.13 shows the time trajectories for the two oscillators for both  $x$ - and velocity couplings. It may be noticed that for velocity coupling the van der Pol oscillator loses some amplitude due to the coupling with the unforced Duffing resonator.

Finally, two diffusively coupled identical van der Pol - Duffing oscillators behave similar to two diffusively coupled van der Pol oscillators, namely, in-phase synchronisation is seen for velocity coupling, while, for  $x$ - coupling, the coupled system exhibits motion in-phase or anti-phase, depending on the initial values.

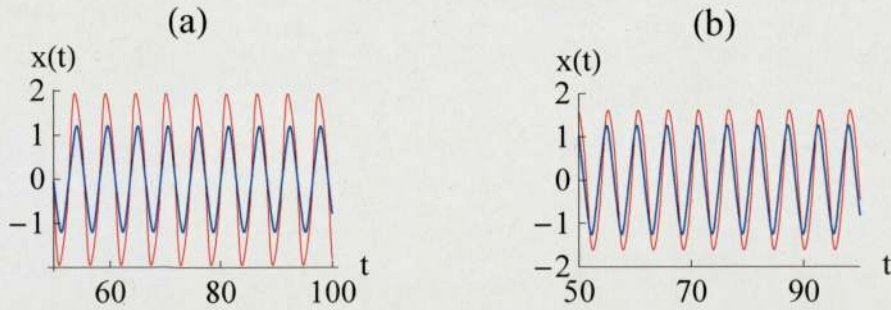


Figure 2.13:  $x$ -coupled (a) and velocity-coupled (b) van der Pol oscillator (red) and Duffing resonator (blue) for  $\rho = \alpha = \beta = \mu = K = 1$  and  $\delta = 0.2$ .

## 2.3 Summary

In this Chapter we presented some properties of single van der Pol oscillator and Duffing resonator and also discussed their relevance to MEMS devices. We also discussed the effect of linear displacement and velocity coupling on the motion of two coupled oscillators. The experiments in this chapter have shown that a range of behaviour can be expected even in the simple case of coupling two dynamical objects together. The condition for in-phase synchronisation for velocity coupled identical van der Pol oscillators was also derived under a perturbation analysis (Section 2.2.1). This same condition has been obtained by Wang and Slotine [1] considering contraction of a single van der Pol oscillator and using Partial Contraction theory. This theory will be discussed in more detail in the next Chapter.

## Chapter 3

# Partial Contraction Theory

In the previous chapter we saw a local analysis, based on linearised perturbation theory, to display the change in behaviour of coupled systems. We now consider a global approach capable of scaling up to chain and networks of oscillators. The concept of contraction is re-visited and extended to networks of coupled oscillators in the next Section, and applied to a ring of four coupled oscillators in Section 3.2. Partial Contraction Theory for general networks is presented in Section 3.3, and the Chapter ends with a short Summary.

### 3.1 Contraction and Partial Contraction

In Section 2.1.1 we discussed that linearisation of the second order differential equation can be compactly written as

$$\dot{\mathbf{x}} = \mathbf{f}(\mathbf{x}, t), \quad (3.1)$$

where  $\mathbf{x} = (x, y)$ , so that Equation (2.3) can be written as

$$\mathbf{F} = \frac{d\mathbf{f}}{d\mathbf{x}}. \quad (3.2)$$

and that the system is said to be contracting, (i.e., all trajectories tend to a single trajectory asymptotically), if all eigenvalues  $\lambda_i$  of the Jacobian  $\mathbf{F}$  are negative, or, alternatively, if  $\mathbf{F}$  is negative definite.

Wang and Slotine, [1], have extended this concept to networks of coupled oscillators, where only part of the system is known to be contracting; Thus consider a system where  $i^{th}$  variable  $\mathbf{x} = (\mathbf{x}_1, \mathbf{x}_2)$  can be considered separately as

$$\dot{\mathbf{x}}_1 - \mathbf{h}(\mathbf{x}_1, \mathbf{t}) = \dot{\mathbf{x}}_2 - \mathbf{h}(\mathbf{x}_2, \mathbf{t}), \quad (3.3)$$

with  $\mathbf{h}(\mathbf{x}, \mathbf{t}) = \mathbf{f}(\mathbf{x}, \mathbf{t}) + \mathbf{u}(\mathbf{x}, \mathbf{t})$ , where  $\mathbf{u}(\mathbf{x}, \mathbf{t})$  refers to the network part of the system; Then, if,  $\mathbf{h}$  is contracting, then  $\mathbf{x}_1$  and  $\mathbf{x}_2$  will converge to each other asymptotically, leading to complete synchronisation. This concept of Partial Contraction Theory can be applied to the case of two identical velocity-coupled van der Pol oscillators considered in Section 2.2.1, as follows: For identical oscillators, Equation (2.18) can be rewritten as:

$$\begin{aligned} \ddot{x}_1 + \mu(x_1^2 + \kappa_1 + \kappa_2 - 1)\dot{x}_1 + \rho x_1 &= \mu(\kappa_2 \dot{x}_1 + \kappa_1 \dot{x}_2), \\ \ddot{x}_2 + \mu(x_2^2 + \kappa_1 + \kappa_2 - 1)\dot{x}_2 + \rho x_2 &= \mu(\kappa_2 \dot{x}_1 + \kappa_1 \dot{x}_2). \end{aligned} \quad (3.4)$$

Therefore, from Appendix B, the system will be contracting and  $\mathbf{x}_1 \rightarrow \mathbf{x}_2$  if  $\kappa_1 + \kappa_2 > 1$ , which is exactly the condition we obtained in Section 2.2.1.

## 3.2 Ring of Four Coupled Oscillators

We apply Partial Contraction Theory to obtain conditions for complete synchronisation in one-way and two-way coupled ring of four oscillators, and use the result to compare the two couplings for a ring of identical van der Pol oscillators.

### 3.2.1 Oscillator Ring with Two-way Coupling

We consider equations of motion for a ring of four two-way coupled oscillators shown below:

From Equation (3.1), the linearised equations for the four oscillators can be written as

$$\dot{\mathbf{x}}_1 - \mathbf{f}(\mathbf{x}_1, t) = \mathbf{u}(\mathbf{x}_4) - \mathbf{u}(\mathbf{x}_1) + \mathbf{u}(\mathbf{x}_2) - \mathbf{u}(\mathbf{x}_1), \quad (3.5)$$

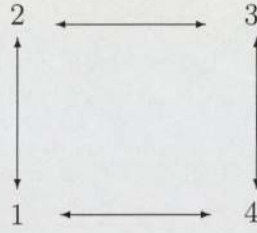


Figure 3.1: A ring of four oscillators with two-way coupling.

$$\dot{\mathbf{x}}_2 - \mathbf{f}(\mathbf{x}_2, t) = \mathbf{u}(\mathbf{x}_1) - \mathbf{u}(\mathbf{x}_2) + \mathbf{u}(\mathbf{x}_3) - \mathbf{u}(\mathbf{x}_2), \quad (3.6)$$

$$\dot{\mathbf{x}}_3 - \mathbf{f}(\mathbf{x}_3, t) = \mathbf{u}(\mathbf{x}_2) - \mathbf{u}(\mathbf{x}_3) + \mathbf{u}(\mathbf{x}_4) - \mathbf{u}(\mathbf{x}_3), \quad (3.7)$$

$$\dot{\mathbf{x}}_4 - \mathbf{f}(\mathbf{x}_4, t) = \mathbf{u}(\mathbf{x}_3) - \mathbf{u}(\mathbf{x}_4) + \mathbf{u}(\mathbf{x}_1) - \mathbf{u}(\mathbf{x}_4), \quad (3.8)$$

where  $\mathbf{u}$  represents the coupling between any two oscillators. The above equations may be rearranged as

$$\dot{\mathbf{x}}_1 - \mathbf{f}(\mathbf{x}_1, t) - 2\mathbf{u}(\mathbf{x}_1) = \dot{\mathbf{x}}_3 - \mathbf{f}(\mathbf{x}_3, t) - 2\mathbf{u}(\mathbf{x}_3) = \mathbf{u}(\mathbf{x}_2) + \mathbf{u}(\mathbf{x}_4) \quad (3.9)$$

$$\dot{\mathbf{x}}_2 - \mathbf{f}(\mathbf{x}_2, t) - 2\mathbf{u}(\mathbf{x}_2) = \dot{\mathbf{x}}_4 - \mathbf{f}(\mathbf{x}_4, t) - 2\mathbf{u}(\mathbf{x}_4) = \mathbf{u}(\mathbf{x}_1) + \mathbf{u}(\mathbf{x}_3) \quad (3.10)$$

Therefore, from Equation (3.3), if  $\mathbf{f}(\mathbf{x}, t) - 2\mathbf{u}(\mathbf{x})$  is contracting, then,  $\mathbf{x}_1 \rightarrow \mathbf{x}_3$  and  $\mathbf{x}_2 \rightarrow \mathbf{x}_4$  asymptotically, so that,

$$\dot{\mathbf{x}}_1 - \mathbf{f}(\mathbf{x}_1, t) - 2\mathbf{u}(\mathbf{x}_1) = 2\mathbf{u}(\mathbf{x}_2) \quad (3.11)$$

$$\dot{\mathbf{x}}_2 - \mathbf{f}(\mathbf{x}_2, t) - 2\mathbf{u}(\mathbf{x}_2) = 2\mathbf{u}(\mathbf{x}_1) \quad (3.12)$$

Once again, the two equations can be rearranged as

$$\dot{\mathbf{x}}_1 - \mathbf{f}(\mathbf{x}_1, t) - 4\mathbf{u}(\mathbf{x}_1) = \dot{\mathbf{x}}_2 - \mathbf{f}(\mathbf{x}_2, t) - 4\mathbf{u}(\mathbf{x}_2) = 2\mathbf{u}(\mathbf{x}_2) + 2\mathbf{u}(\mathbf{x}_2) \quad (3.13)$$

Therefore, once again from Equation (3.3),  $\mathbf{x}_1 \rightarrow \mathbf{x}_2$  asymptotically if  $\mathbf{f}(\mathbf{x}, t) - 4\mathbf{u}(\mathbf{x})$  is contracting. Hence, the sufficient condition for the network to synchronise is that

$$\mathbf{f}(\mathbf{x}, t) - 2\mathbf{u}(\mathbf{x}) \quad (3.14)$$

is contracting.

### 3.2.2 Oscillator Ring with One-way Coupling

Next we consider a condition for total synchronisation in a ring of four oscillators with one-way coupling, as illustrated in the figure below:

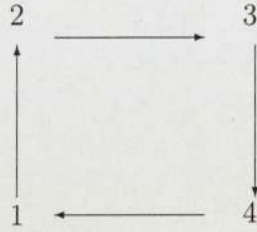


Figure 3.2: A ring of four oscillators with one-way coupling.

In order to proceed with the analysis for this system, we need to consider another aspect of Partial Contraction Theory, namely, building an auxiliary system  $\mathbf{f}(\mathbf{y})$  to the original system of oscillators [1]. Equations of motion for the oscillators can be written as

$$\dot{\mathbf{x}}_i = \mathbf{f}(\mathbf{x}_i, \mathbf{t}) + \mathbf{K}(\mathbf{x}_{i+1} - \mathbf{x}_i) \quad i = 1, 2, 3, 4 \quad (3.15)$$

where,  $\mathbf{K} > 0$  is the coupling between the oscillators, and the subscripts are calculated circularly. The system is equivalent to

$$\dot{\mathbf{x}}_i = \mathbf{f}(\mathbf{x}_i, \mathbf{t}) - \mathbf{K}(2\mathbf{x}_i + \mathbf{x}_{i+1} + \mathbf{x}_{i+2}) + \mathbf{K} \sum_{i=1}^4 \mathbf{x}_i, \quad (3.16)$$

so that an auxiliary system can be constructed:

$$\dot{\mathbf{y}}_i = \mathbf{f}(\mathbf{y}_i, \mathbf{t}) - \mathbf{K}(2\mathbf{y}_i + \mathbf{y}_{i+1} + \mathbf{y}_{i+2}) + \mathbf{K} \sum_{i=1}^4 \mathbf{x}_i \quad (3.17)$$

For the auxiliary system to admit to a particular solution  $y_1 = y_2 = y_3 = y_4 = y_\infty$ , we study the Jacobian matrix of the auxiliary system, [1]:

$$J = \begin{pmatrix} F_1 - 2K & -K & -K & 0 \\ 0 & F_2 - 2K & -K & -K \\ -K & 0 & F_3 - 2K & -K \\ -K & -K & 0 & F_4 - 2K \end{pmatrix},$$

CHAPTER 3. PARTIAL CONTRACTION THEORY

where  $\mathbf{F}_i = \frac{df_i(\mathbf{y}, t)}{d\mathbf{y}}$ . Then the symmetric part of the Jacobian can be written as

$$\mathbf{J}_s = \mathbf{I}_{F_{is}}^4 - \frac{1}{2}\mathbf{U}_K^4 - \frac{1}{2}\mathbf{J}_+ \quad (3.18)$$

where

$$I_{F_i}^4 = \begin{pmatrix} F_{1s} - K & 0 & 0 & 0 \\ 0 & F_{2s} - K & 0 & 0 \\ 0 & 0 & F_{3s} - K & 0 \\ 0 & 0 & 0 & F_{4s} - K \end{pmatrix}, \quad (3.19)$$

$$U_K^4 = \begin{pmatrix} K & K & K & K \\ K & K & K & K \\ K & K & K & K \\ K & K & K & K \end{pmatrix}, \quad \text{and} \quad J_+ = \begin{pmatrix} K & 0 & K & 0 \\ 0 & K & 0 & K \\ K & 0 & K & 0 \\ 0 & K & 0 & K \end{pmatrix}. \quad (3.20)$$

The system considered will evolve to complete synchronisation if the symmetric part of the Jacobian of the system,  $J_s$ , is contracting. Since  $\mathbf{K} > 0$ , so that,  $U_K^4, J_+ > 0$ , it may be seen from Equation (3.18) that  $J_s$  will be negative definite if  $I_{F_{is}}^4$  is negative definite. Thus, a sufficient condition for complete synchrony for a ring of one-way coupled oscillators is that

$$\mathbf{F}_{is} - \mathbf{K} < 0. \quad (3.21)$$

From Equation (3.21) and Appendix B, it can be seen that a ring of four one-way velocity - coupled van der Pol oscillators will converge to the same trajectory if  $\mathbf{K} > 1$ ; From Equation (3.14) and Appendix B, on the other hand, we see that the condition  $\mathbf{u} > \frac{1}{2}$  is sufficient for a two-way coupled ring of van der Pol oscillators to synchronise completely. Therefore, two-way diffusive coupling is more efficient in inducing complete synchronisation in a ring of four velocity - coupled van der Pol oscillators; this is shown in Figure 3.3 for  $\mu = 1$  and  $\kappa = 1.1$ , where the ring of van der Pol oscillators with two-way coupling reaches synchronisation before the ring of one-way coupled oscillators.

So far, the conditions for complete synchrony were obtained in terms of the contraction of the Jacobian of the system within the framework of the Partial Contraction

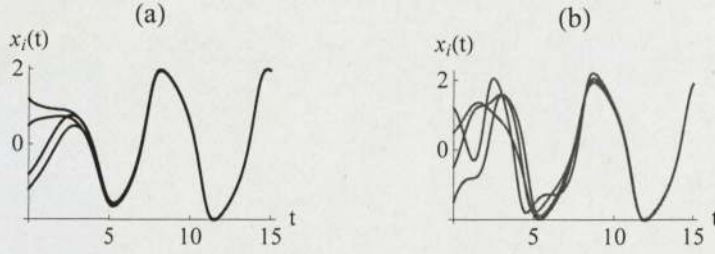


Figure 3.3: Time trajectories for a ring of four velocity-coupled van der Pol oscillators with (a) two-way coupling, and, (b) one-way coupling.

theory. From the discussion at the end of Subsection 2.2.1 we have seen that for a system to be contracting, the real part of the eigenvalues of its Jacobian should be negative, which is mainly determined by the trace of the Jacobian matrix. In the next section we present an extension of the theory to general networks, where the condition for synchrony is in terms of the eigenvalues of the Jacobian of the oscillator system and that of the network, which would depend on the full symmetric Jacobian.

### 3.3 Networks with General Structures

We extend the analysis of Subsection 3.2.2 to a general network of oscillators coupled through linear diffusive term  $\mathbf{K}_{ij}$  connecting nodes  $i$  and  $j$  in the network. It is also assumed that the coupling is bi-directional and symmetric and positive definite, i.e.,  $\mathbf{K}_{ij} = \mathbf{K}_{ji} > \mathbf{0}$ . Then a network of  $n$  oscillators is represented as

$$\dot{\mathbf{x}}_i = \mathbf{f}(\mathbf{x}_i, t) + \sum_{j \in N_i} \mathbf{K}_{ij}(\mathbf{x}_j - \mathbf{x}_i), \quad (3.22)$$

where  $N_i$  denotes the indices of the active links in the network, An auxiliary system can be constructed as

$$\dot{\mathbf{y}}_i = \mathbf{f}(\mathbf{y}_i, t) + \sum_{j \in N_i} \mathbf{K}_{ij}(\mathbf{y}_j - \mathbf{y}_i) - \mathbf{K} \sum_{j=1}^n \mathbf{y}_j + \mathbf{K} \sum_{j=1}^n \mathbf{x}_j, \quad (3.23)$$

Once again, we are interested in the particular solution,  $y_1 = y_2 = \dots = y_n = y_\infty$ , and compute  $J_s$ , the symmetric part of the Jacobian for the auxiliary system, [1] [45], as

$$\mathbf{J}_s = \mathbf{I}_{F_{is}}^n - \mathbf{U}_K^n - \mathbf{L}_K, \quad (3.24)$$

## CHAPTER 3. PARTIAL CONTRACTION THEORY

where  $\mathbf{L}_K$  is similar to the symmetric part of the weighted Laplacian in the graph theory, and is defined as  $\mathbf{L} = \sum_{i,j \in N_i} \mathbf{T}_{Kij}^n$ , where

$$\mathbf{T}_{K}^n = \begin{bmatrix} \ddots & \vdots & & \vdots & \\ \cdots & K & \cdots & K & \cdots \\ & \vdots & \ddots & \vdots & \\ \cdots & K & \cdots & K & \cdots \\ & \vdots & & \vdots & \ddots \end{bmatrix}_{n \times n} \quad (3.25)$$

It can be shown that, [1],[45], that the network of oscillators will achieve global synchronisation if

$$\lambda_{\min}(\mathbf{L}) > \lambda_{\max}(\mathbf{F}_{is}), \quad (3.26)$$

where,  $\lambda$  are eigenvalues of the corresponding matrices. *Thus, if the eigenvalues associated with the MEMS resonator in the network have an upper bound, one can always find coupling strengths which will satisfy Equation (3.26), leading to complete synchronisation of the whole network system.*

### 3.4 Summary

We have presented the concept of Partial Contraction Theory when a part of the network is contracting, which is determined mostly by the trace of the Jacobian matrix of the part of the system. We also presented Partial Contraction theory for a general network of oscillators, and, the condition for total synchrony was obtained in terms of its eigenvalues, which is a more general property of the matrices representing the system. We found that if eigenvalues associated with the MEMS resonator in the network have an upper bound, a critical coupling strength exists above which the whole network would evolve to complete synchrony. However, Partial Contraction theory can only be applied to study complete synchronisation and only for a network of identical oscillators. In the next Chapter we consider one-dimensional chains of linear oscillators, and some of the results will be discussed in terms of the theory.

# Chapter 4

## Chain of Identical Oscillators

In this Chapter we consider the motion of one-dimensional coupled chains of simple oscillators, beginning with a mass on a spring in Section 4.1. In the next Section we consider a more complex dynamical system, a chain of van der Pol oscillators having non-linear damping but linear spring constant. In Section 4.3, we extend our consideration to include a non-linear spring constant. For both these cases we consider both diffusive  $x$ - and velocity- coupling, restricting ourselves to the nearest-neighbour interaction. For some parameter values, complete synchronisation is achieved in both cases, and is analysed in terms of the Partial Contraction Theory in Section 4.5.

### 4.1 Linear Oscillators: Fermi Pasta Ulam Model

The frequency spectrum of a chain of linear oscillator which are coupled linearly is constant in time; However, the addition of a weak non-linear coupling term leads to a number of interesting phenomena such as redistribution of energy from the initial mode [46] and formation of soliton-like breathers [47]. The Hamiltonian describing the motion of masses  $m_i$ , coupled through nonlinear spring, may be written as [48]

$$H = \sum_{i=1}^n \left[ \frac{p_i^2}{2m_i} + \frac{1}{2}(x_{i+1} - x_i)^2 + \frac{\eta}{\nu + 1}(x_{i+1} - x_i)^{\nu+1} \right], \quad (4.1)$$

where  $\eta$  is the strength of the non-linear coupling, and  $\nu$  is either 2 or 3. The corresponding coupled differential equation for the  $i^{\text{th}}$  oscillator can be written as

$$\ddot{x}_i = (x_{i+1} + x_{i-1} - 2x_i) + \eta((x_{i+1} - x_i)^\nu - (x_i - x_{i-1})^\nu), \quad (4.2)$$

Below we discuss some interesting solutions of Equation (4.2) when the initial displacement of the oscillators in the chain is in the lowest mode (Section 4.1.1), or in the highest mode (Section 4.1.2).

### 4.1.1 Fermi Pasta Ulam Paradox

The Fermi Pasta Ulam (FPU) problem is named after the three scientists [49], who over fifty years ago together with Mary Tsingou, used a computer to solve Equation 4.2 numerically. It was expected that when the chain of non-linearly coupled linear oscillators was initially in its lowest ( $\alpha$ ) mode, shown in Figure 4.1 (b), high-frequency modes would appear and the initial energy would eventually be almost equipartitioned. However, when they let the program run overnight (accidentally!), they found that, after remaining in the state of equipartition for some time, the system moved away from it, and, after 157 cycles of equipartition, returned to the initial mode with almost 97% efficiency [46]. Figure 4.1 (a) shows the transfer of energy to a higher mode, which almost returns to the initial mode (Figure 4.1 (b)).

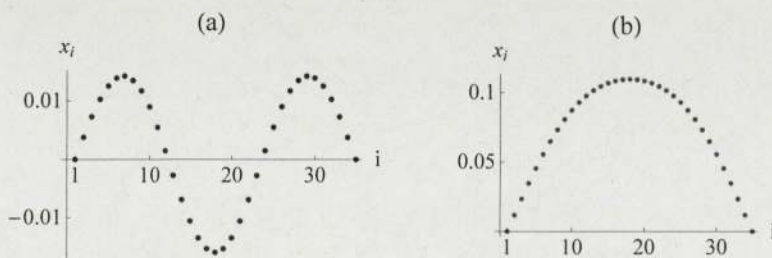


Figure 4.1: Displacement of simple oscillators in a chain with non-linear coupling index  $\nu = 3$ , and coupling constant  $\eta = 0.5$ : (a) at  $t=6030$ , and (b) at  $t=0$  and  $t=6031$ .

Not only was the above work instrumental in starting a new field of ‘Numerical Experiment’, but has also been at the origin of the concept of solitons [46] and Discrete Breathers (DB), which are discussed below.

### 4.1.2 Discrete Breathers

Discrete breathers (DBs), also known as Intrinsic Localised Modes (ILMs) [50], are spatially localised and time-periodic excitations in non-linear lattices. They can be odd or even, i.e., the displacements of the oscillators is anti-symmetric or symmetric about the zero axis [47]. In FPU lattices, DBs can form when the chain, initially in the high-frequency ( $\beta$ ) mode, Figure 4.2 (a), follows a path to equipartition. This is a kind of Anti-FPU problem, where we begin with the short wavelength mode, instead of the long-wavelength one. Formation of odd, even and combination modes is illustrated in Figures 4.2 (b) - (d) for cubic coupling and  $\eta = 0.05$ .

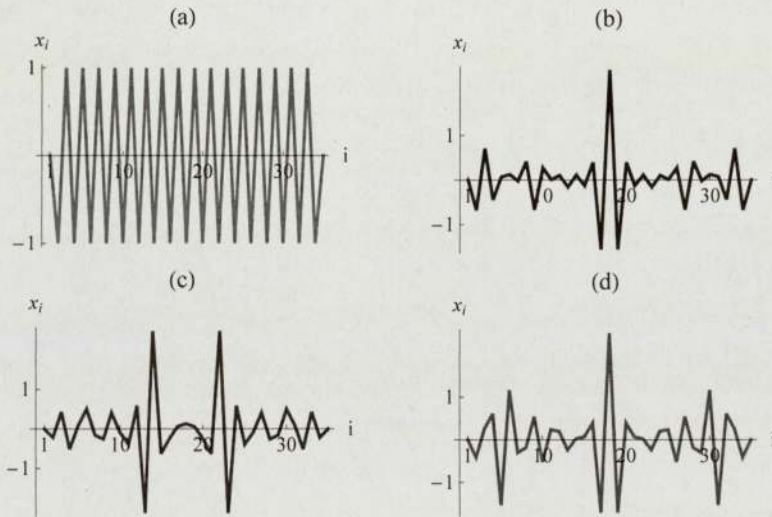


Figure 4.2: Formation of discrete breathers in a chain of linear oscillators where  $\nu = 3$ , and, the non-linear coupling strength  $\eta = 0.05$ : (a) Initial displacement of the chain of oscillators in the  $\beta$  mode, (b) odd- mode breather ( $t = 565$ ), (c) two coupled even-mode breathers ( $t = 810$ ), and, (d) an odd- mode breather surrounded by even- mode breathers ( $t = 650$ ).

These DBs or ILMs have energy profiles resembling those of localised defect/impurity modes in a harmonic lattice, but, like solitons, they can move. Therefore, ILMs could be used to study the stabilisation of an arrays of MEMS resonators, in line with the use of a travelling pulse to study the stabilisation of arrays of actuators and sensors [51]. Discrete breathers have also been studied experimentally in nonlinear electric transmission line arrays [52]. Sato et al. [53] have presented a detailed study of ILMs

in MEMS arrays with Duffing-like on site nonlinearity combined with inter-site cubic nonlinearity in monatomic and diatomic lattices; They find that, for their arrays of MEMS cantilevers, while both on-site and inter-site nonlinearities lead to localisation, inter-site nonlinearity provides greater energy localisation, since, inter-site nonlinearity is about two orders of magnitude larger for their MEMS arrays.

## 4.2 Dynamic Systems: Chain of van der Pol Oscillators

As discussed in Chapter 2, the van der Pol oscillator admits self-sustained oscillations. Therefore, it can be used to drive a collection of Duffing resonators, whose amplitude would otherwise decay to zero in the absence of an external force. In Section 4.3, we consider a chain of identical (unforced) Duffing resonators with *non-linear damping* (van der Pol-Duffing oscillator described by Equation (2.8)), and, in Chapter 5 we consider the hybrid case of Duffing resonators driven by van der Pol oscillators. In this section we present results for chains of van der Pol oscillators coupled through their displacements or their velocities. For all these cases, we consider a chain of 32 units with two-way linear diffusive coupling. Unlike the FPU model (Section 4.1), the initial oscillator values are set randomly and the coupled differential equations have been solved numerically for floating boundary condition. In addition to the time trajectories of the chains of oscillators, some of the results will be presented in terms of a measure of synchronisation,  $C_s$ ; this will be especially useful for comparing the effect of oscillator parameters and coupling constants on the level of synchronisation reached.

### 4.2.1 Measures of Synchronisation

In addition to complete synchronisation (CS) and being totally unsynchronised, the network of oscillators could be in one of many states of (partial) synchronisation, such as: *General synchronisation* [54], *phase synchronisation* [55] [56], where the oscillators

move with the same phase but with different amplitudes. The collection of coupled oscillators could also exhibit *lag-synchronisation* [18], or be *phase-locked*, where, although oscillators are not moving with the same phase, their phase difference with each other remains constant with time [57] [58]. A special case for the latter is *anti-phase locked synchronisation*: We saw an example of this for two  $x$ -coupled van der Pol oscillators (Figure 2.8); For the case of a chain of oscillators, anti-phase locking would imply that there are two groups of oscillators which are in complete synchrony with each other and anti-phase-locked with the other group.

Just as there are many forms of synchronisation, there are many measures of synchronisation suggested in the literature [59] [60], most of them for the system of two-coupled oscillators. In order to compare the level of entrainment in chains of different systems and for different coupling constants, we define a measure of synchronisation as: [61]

$$C_{sync} = \frac{\langle \bar{x}^2 \rangle - \langle \bar{x} \rangle^2}{\frac{1}{n} \sum_i^n (\langle x_i^2 \rangle - \langle x_i \rangle^2)}, \quad \text{where } \bar{x} = \sum_i^n \langle x_i \rangle, \quad (4.3)$$

where,  $n$  is the number of oscillators in the chain,  $\langle \dots \rangle$  represents the time average, and  $x_i$  could represent the displacement or the phase of the  $i^{th}$  oscillator.

### 4.2.2 Velocity Coupling

We first consider a chain of velocity-coupled van der Pol oscillators: The equation of motion for the  $i_{th}$  van der Pol oscillator is:

$$\begin{aligned} \ddot{x}_1 + \mu(x_1^2 - 1)\dot{x}_1 + \rho x_1 &= \mu\kappa(\dot{x}_2 - \dot{x}_1) \\ \ddot{x}_i + \mu(x_i^2 - 1)\dot{x}_i + \rho x_i &= \mu\kappa(\dot{x}_{i+1} + \dot{x}_{i-1} - 2\dot{x}_i) \quad i = 2, 31 \\ \ddot{x}_{32} + \mu(x_{32}^2 - 1)\dot{x}_{32} + \rho x_{32} &= \mu\kappa(\dot{x}_{31} - \dot{x}_{32}). \end{aligned} \quad (4.4)$$

For simplicity, we have chosen  $\rho = 1$  for all the results presented in this work, unless otherwise stated. Since the initial state of the 32 oscillators is assigned randomly, the initial motion of the oscillators is practically uncorrelated to each other; This is illustrated in Figure 4.3, where the displacement of each oscillator at  $t = 0$  is also

shown. However, soon a cooperative motion of oscillators emerges, as shown in Figure 4.4.

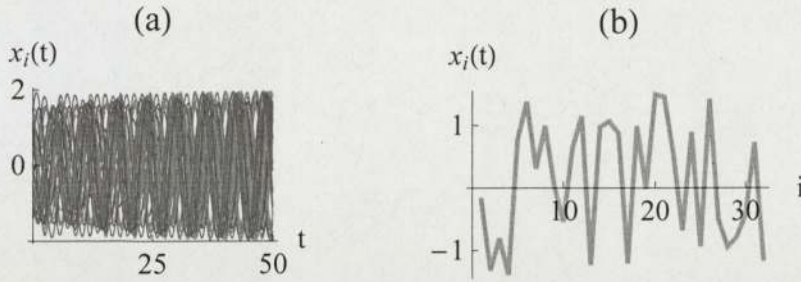


Figure 4.3: (a) Time-dependence of the displacement of the 32 velocity-coupled van der Pol oscillators, and, (b) oscillator displacement along the chain for  $t=0$ .

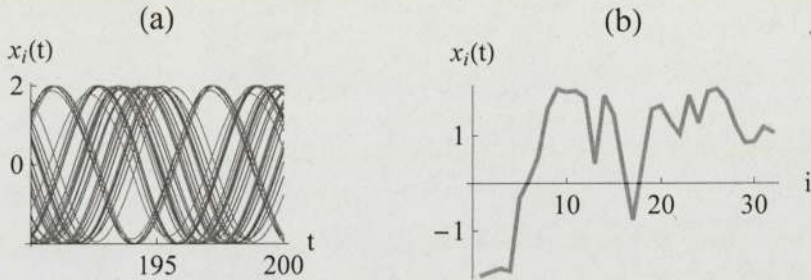


Figure 4.4: Time-dependence of the displacement of a chain of 32 velocity-coupled van der Pol oscillators showing emergence of cooperative behaviour: (a) time trajectories and (b) oscillator displacement along the chain for  $t=200$ .

For the case of velocity coupling, total synchronisation is almost always achieved asymptotically; This is illustrated in Figure 4.5, where almost complete synchronisation is obtained for  $\mu = \kappa = 0.1$  for  $t \approx 10000$ , where the net coupling between the oscillators is very small ( $\mu\kappa = 0.01$ ). The corresponding phase portrait for the 32 oscillators is presented in Figure 4.6, which shows that the phase portrait of all the oscillators converges to a single limit cycle.

We have used the measure of synchronisation defined above (Equation (4.3)) to calculate the time  $t_s$  needed to achieve 90 % synchronisation, ( $C_s = 0.9$ ), for various values of  $\mu$  and  $\kappa$ . Figure 4.7 shows the variation of  $t_s$  with the relative coupling constant  $\kappa$  for different values of  $\mu$ . From Figure 4.7, one can easily see that time needed

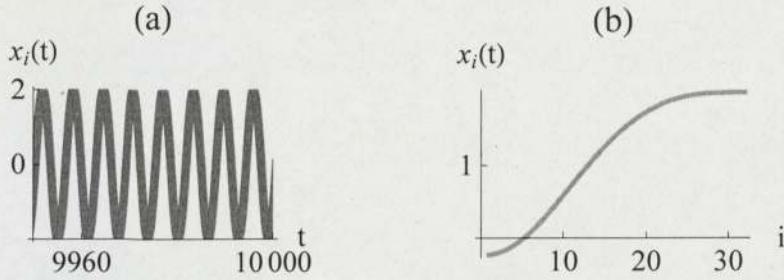


Figure 4.5: (a) Time-dependence of the displacement of the 32 velocity-coupled van der Pol oscillators, and (b) oscillator displacement along the chain for  $t=99700$ .

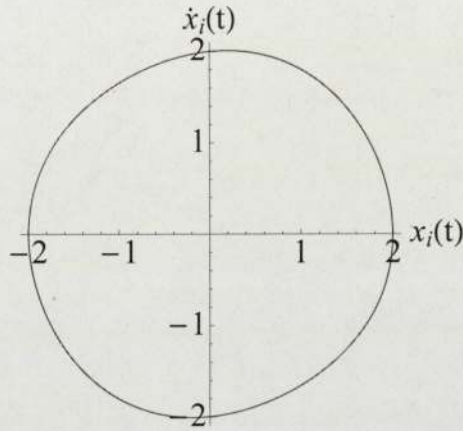


Figure 4.6: Phase portrait of the 32 velocity-coupled van der Pol oscillators ( $\mu = \kappa = 0.01$ ).

to reach CS decreases as the (relative) coupling constant  $\kappa$  increases; This is to be expected. However, from the figure it is also apparent that the rate of synchronisation depends on the nonlinear damping parameter  $\mu$ : synchronisation is achieved more rapidly as  $\mu$  increases. In agreement with Wang and Slotine [1], we find that it is the relative coupling constant  $\kappa$ , rather than total coupling  $\mu\kappa$ , which is relevant for comparison purposes. A more detailed discussion of our results in the context of the Partial Contraction theory will be presented in Section 4.5.

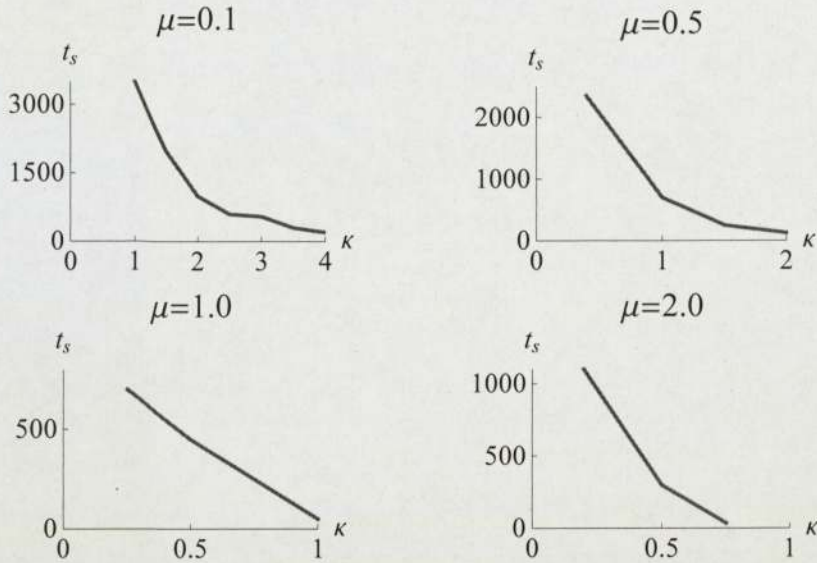


Figure 4.7: Variation of  $t_s$ , time needed to achieve 90% synchronisation ( $C_s = 0.9$ ), with the coupling constant  $\kappa$  for various values of  $\mu$  in velocity-coupled chains of van der Pol oscillators;  $C_s$  was calculated using Equation (4.3).

### 4.2.3 Displacement Coupling

We next consider a chain of  $x$ -coupled van der Pol oscillators, governed by the equation

$$\begin{aligned}
 \ddot{x}_1 + \mu(x_1^2 - 1)\dot{x}_1 + \rho x_1 &= \mu k(x_2 - x_1) \\
 \ddot{x}_i + \mu(x_i^2 - 1)\dot{x}_i + \rho x_i &= \mu k(x_{i+1} + x_{i-1} - 2x_i) \quad i = 2, 31 \\
 \ddot{x}_{32} + \mu(x_{32}^2 - 1)\dot{x}_{32} + \rho x_{32} &= \mu k(x_{31} - x_{32}),
 \end{aligned} \tag{4.5}$$

where, once again,  $\rho = 1$ . The motion of the oscillators is random in the beginning, similar to Figure 4.3; Unlike the case for velocity coupling, total synchronisation is *generally not* observed for displacement coupling. In Figure 4.8, we present the time trajectories and oscillator displacement for  $\mu = 0.1$  and total coupling constant  $k = 2$ . For this case, it is seen that the oscillators in the chain arrange themselves into roughly 3 groups, two groups which are almost totally synchronised within themselves but anti-phase locked with each other; The motion of the third group of oscillators is somewhat non-cooperative. We have observed that once the pattern of synchronisation is established, it does not change with time. The same behaviour is seen for other coupling constants for  $\mu = 0.01$ . Thus for this case, calculating  $C_s$  using oscillator

phases is more pertinent. Oscillator phase, in general, is calculated using the Hilbert Transform; however, since the limit cycles for the coupled system are seen to encircle the origin in the phase plane, we have used the following definition for calculating the oscillator phases [18]

$$\theta_i(t) = \arctan \left( \frac{\dot{x}_i(t)}{x_i(t)} \right). \quad (4.6)$$

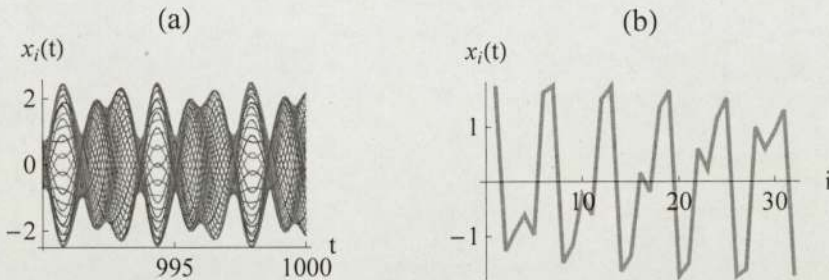


Figure 4.8: (a) Time trajectories, and, (b) oscillator displacement for  $x$ -coupled chain of van der Pol oscillators for  $\mu = 0.1$  and total coupling  $\mu\kappa = 2$ .

We have also solved Equation 4.6 for  $\mu = 0.5, 1$  and  $2$ ; In all these cases, the 32 oscillators are seen to form two groups, one which has all oscillators within the group more-or-less ( $x$ )-synchronised with each other, while the remaining oscillators are unsynchronised. In these cases, it is more useful to consider oscillator displacement while calculating the corresponding measure of synchronisation,  $C_s$ . The dependence of  $C_s$  on the coupling constant for the four cases is shown in Figure 4.9, where, unlike the case for velocity coupling, the level of synchronisation for  $x$ -coupling is much less dependent on the coupling constant.

### 4.3 Dynamic System with Added Nonlinear Spring Constant

In Section 4.1 we considered the behaviour of one-dimensional chains of linear oscillators, identical masses on a spring, while, in Section 4.2, we discussed the effect of adding some internal dynamics to the oscillator in the form of non-linear damping term; In this Section, we discuss the effect of adding a non-linear (cubic) spring constant to

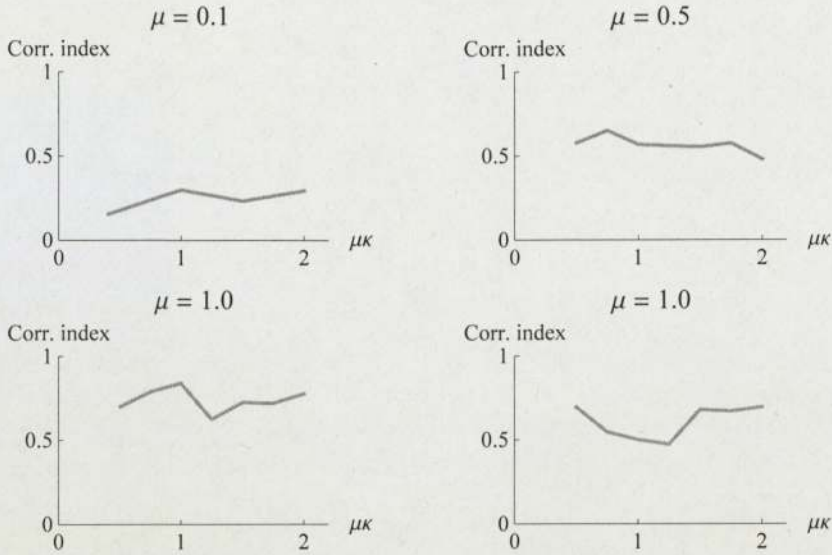


Figure 4.9: The measure of phase synchronisation ( $\mu = 0.1$ ), and, displacement synchronisation ( $\mu = 0.5, 1$  and  $3$ ), plotted against the (total) coupling constant  $\mu\kappa$  for a chain of  $x$ - coupled van der Pol oscillators.

this dynamical system. The coupled equations of motion for this van der Pol - Duffing system are:

$$\ddot{x}_i + \mu(x_i^2 - 1)\dot{x}_i + \rho x_i + \beta x_i^3 = \mu\kappa(\dot{x}_{i+1} + \dot{x}_{i-1} - 2\dot{x}_i) + \mu k(x_{i+1} + x_{i-1} - 2x_i) \quad i = 1, 32, \quad (4.7)$$

where, once again,  $\mu k$  and  $\mu\kappa$  are the  $x$ - and velocity coupling strengths, respectively, and both ends of the chain are free. For the trivial case of  $\mu = 0$ , no emergent behaviour is seen for the  $x$ -coupling, while, the velocity coupling results in the oscillators' amplitudes decaying to 0. For this Section, we once again assume  $\rho = 1$ .

### 4.3.1 Velocity Coupling

The dynamics of the velocity-coupled chain of identical van der Pol - Duffing oscillators is obtained by numerically evaluating Equation 4.7 with  $k = 0$ . In general total synchronisation is achieved asymptotically, similar to the case of the velocity-coupled chain of van der Pol oscillators. However, exceptions have been encountered for some combinations of  $\mu, \beta$  and  $\kappa$ , where the oscillator chain fails to synchronise completely. This is illustrated in Figure 4.10, where complete synchronisation is obtained for  $\mu = 0.1$ ,

$\kappa = 4$  and  $\beta = 0.1$  while low synchronisation is seen for  $\mu = 0.1$ ,  $\kappa = 4$  and  $\beta = 0.25$ . In fact, the time trajectories of Figure 4.10 (b) are very similar to the time trajectories for  $x$ -coupled van der Pol oscillators with  $\mu = 0.1$ , Figure 4.8 (a).

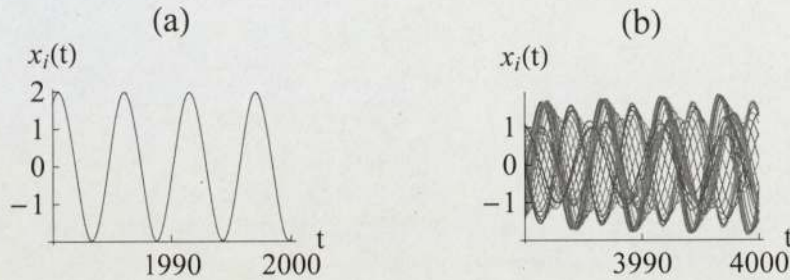


Figure 4.10: Time trajectories of velocity-coupled identical van der Pol - Duffing oscillators with  $\mu = 0.1$ ,  $\kappa = 4$ , (a) showing complete synchronisation for  $\beta = 0.1$  and (b) incomplete synchronisation for  $\beta = 0.25$ .

### 4.3.2 Displacement Coupling

For the case of oscillators coupled through displacement, we substitute  $\kappa = 0$  in Equation (4.7); Unlike the  $x$ -coupled chains of van der Pol oscillators (Subsection 4.2.3), where complete synchronisation is not achieved in general, *addition of the cubic spring constant results in total asymptotic synchronisation* of the oscillators, even for weakly coupled chains. This is illustrated in Figure 4.11.

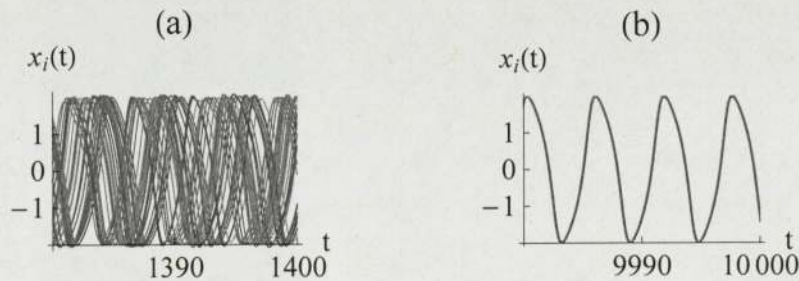


Figure 4.11: Evolution of complete synchronisation for a chain of  $x$ -coupled identical van der Pol - Duffing oscillators for  $\mu = 1$ ,  $\beta = 0.1$  and coupling constant  $k = 0.1$ .

In order to study the effect of the non-linear spring constant  $\beta$  on the rate of synchronisation, we have calculated the minimum relative coupling constant  $k$ ,  $k_{min}$ ,

needed to reach 90 % synchronisation ( $C_s = 0.9$ ), for various values of  $\beta$  and  $\mu$ . It is

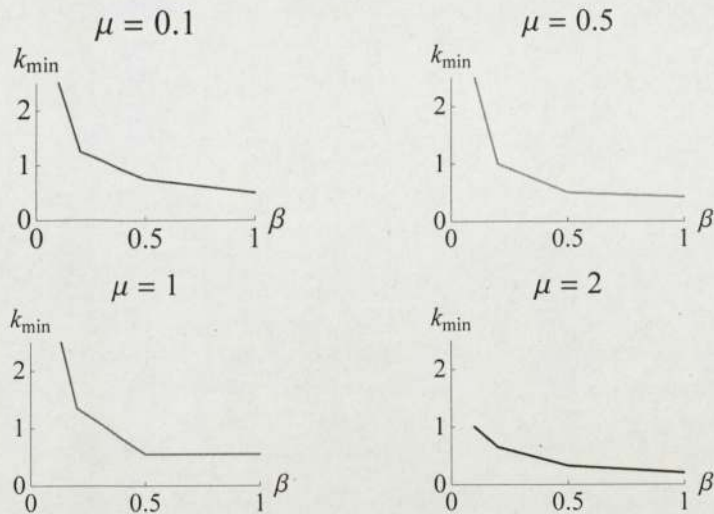


Figure 4.12: Minimum coupling constant  $k$  required for 90 % synchronisation ( $C_s = 0.9$ ) by  $t=1000$ , vs  $\beta$ , in chains of  $x$ - coupled van der Pol - Duffing oscillators, for various values of  $\mu$ , .

seen that, for all  $\mu$ , the coupling strength needed to achieve synchronisation decreases as  $\beta$  increases.

## 4.4 Effect of Frequency Distribution

So far, we have assumed all oscillators to have identical frequencies and obtained complete synchronisation in 3 out of 4 cases discussed: chains of both  $x$ - and  $\dot{x}$ - coupled identical van der Pol - Duffing oscillators, and, chains of velocity-coupled van der Pol oscillators. In the real world, it is difficult for all real oscillators in a network to have the same frequency. Osipov and Sushchic, [62], have compared the effect of the spatial distribution of frequencies along the oscillator array: They found that, keeping the total frequency range constant, the level of synchronisation increased significantly when the frequency distribution was changed from ‘a monotonically varying along the array’- one to the one with irregular variation. In this Section we discuss the effect on synchronisation when the frequencies are allowed to vary randomly within 20% of the set frequency, e.g.,  $\rho = 1 \pm 0.1$ .

Though not complete synchronisation, for all the three cases, a high degree of entrainment is seen for some combination of oscillator parameters and coupling constants; This is illustrated in Figures 4.13 and 4.14.

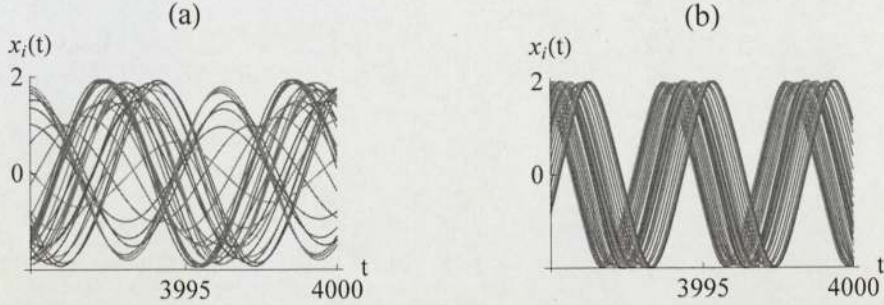


Figure 4.13: Time trajectories for  $\mu = 0.1$ , relative coupling constant  $\kappa(k) = 2$  and 20% frequency spread: (a) velocity-coupled van der Pol oscillators, and (b)  $x$ -coupled van der Pol - Duffing oscillators with  $\beta = 0.5$ . The velocity coupled chain of van der Pol - Duffing oscillators shows unsynchronised motion for these parameters.

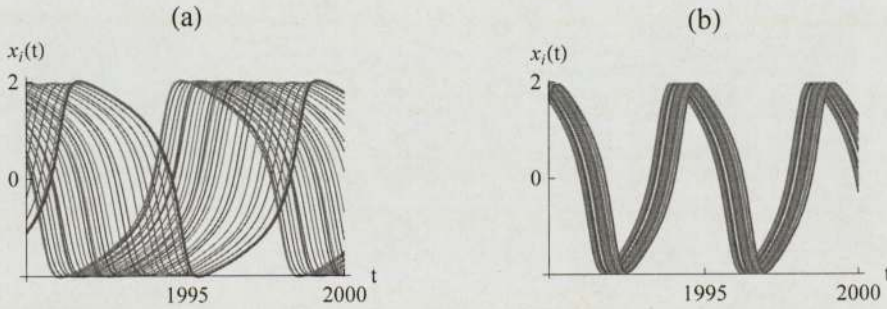


Figure 4.14: Time trajectories for  $\mu = 1$ , relative coupling constant  $\kappa(k) = 0.5$  and 20% frequency spread: (a) velocity-coupled van der Pol oscillators, and (b) velocity-coupled van der Pol - Duffing oscillators with  $\beta = 0.5$ . The  $x$ -coupled chain of van der Pol - Duffing oscillators shows less synchronisation for these parameters.

## 4.5 Comparison with Partial Contraction Theory

Finally, in this Chapter, we compare our results with Partial Contraction theory [1]. The theory has been applied to obtain conditions for complete synchronisation in networks of identical oscillators. (A brief review of Partial Contraction Theory was presented in Chapter 3.) For networks of van der Pol oscillators, the theory has been used

to obtain the minimum coupling needed to achieve asymptotic complete synchronisation, and, in its general form, the theory involves the symmetric form of the Jacobian of the system. For chains of velocity-coupled van der Pol oscillators, Partial Contraction Theory predicts that complete synchronisation is reached if  $\kappa > 1$ . [63] This is in contrast to the results presented in Section 4.2, where the motion of a chain of velocity coupled van der Pol oscillators always resulted in complete synchronisation asymptotically. Also, their analysis does not comment on the effect of  $\mu$  on synchronisation, whereas, our calculations show such a dependence (Figure 4.7).

In Subsection 2.2.1 we presented an analysis of two velocity-coupled van der Pol oscillators in terms of the linear perturbation around the equilibrium point  $(x_1, \dot{x}_1, x_2, \dot{x}_2) = (0,0,0,0)$  and derived the condition  $\kappa_1 + \kappa_2 > 1$  for contraction and thus total synchronisation; The same condition was obtained in Section 3.1 using the global theory of Partial Contraction. However, we can also consider the perturbation of the system about the stable limit cycle [64]. For small  $\mu$ , behaviour of the  $i^{th}$  van der Pol oscillator can be approximated by a sinusoidal trajectory  $x_i = A \cos(\Omega t - \Phi)$ , where  $A = 2$ , and,  $\Omega$  and  $\Phi$  are the frequency and phase of the oscillator. Thus, a linear perturbation analysis of the system represented by Equations (4.5), about the limit cycle, gives that complete synchronisation will be achieved for all  $\kappa > 0$  (Appendix C). A similar condition was obtained by Enjieu Kadji et al. [64] for an  $x$ -coupled ring of four van der Pol oscillators, where the stability analysis predicted total synchronisation for coupling constant  $> 0$ ; However, their numerical simulations showed regions of instability even when this condition was satisfied. Therefore, although some of our numerical experiments result in total synchronisation for coupling constants for which Partial Contraction theory predicts otherwise, there could be regions of instability in the vicinity of this parameter space. Partial Contraction Theory, on the other hand, gives condition for synchronisation *for the whole parameter space*.

In Chapter 3, (Sections 3.3 and 3.4), we mentioned that a critical coupling strength for a network of MEMS could always be found above which the network synchronised completely if there was an upper bound for the eigenvalues associated with the MEMS

unit. Our numerical experiments show that it is possible to achieve asymptotic synchronisation for some parameter space even when the coupling is weaker.

As a corollary, from Equations (2.6) and (2.9), we see that a linear perturbation expansion around the equilibrium point  $(x_i, \dot{x}_i) = (0, 0)$  would lead to the same characteristic equations for both the van der Pol and the van der Pol-Duffing oscillators, leading to similar contraction properties. However, since van der Pol-Duffing oscillator also exhibits a limit cycle behaviour (Figure 2.5), linear perturbation around their respective limit cycles would result in different Jacobian matrices, and therefore different eigenvalues, for the two oscillators, thus possibly accounting for the difference in synchronisation characteristics for the chains of the two systems.

## 4.6 Summary

In this Chapter we studied the behaviour of chains of identical oscillators, and, starting with linear oscillators, explored the effects of adding internal complexities to these oscillators: For chains of linear oscillators, we found that nonlinear coupling of oscillators lead to interesting behaviour such as Fermi-Pasta-Ulam paradox and intrinsic localised modes, with potential application for studying nonlinearities in MEMS arrays. We then added nonlinear damping to these oscillators (van der Pol oscillators) and found that even linear coupling resulted in interesting features like total synchronisation for velocity-coupled chains but not for chains with  $x$ -coupling. However, the addition of a nonlinear (cubic) spring constant term resulted in oscillator synchronisation for  $x$ -coupling as well. In the next chapter we consider coupling oscillators with nonlinear damping (van der Pol oscillator) with oscillators with nonlinear spring constant (Duffing resonator), and, present results for these hybrid chains.

# Chapter 5

## Chains of Coupled Hybrid Oscillators

In chapters 1 and 2, we saw that the Duffing resonator is important in understanding the nonlinear behaviour of many MEMS devices and that some of Duffing oscillator's nonlinear properties could be used for enhancing the device performance, such as, use of frequency mixing near the onset of Duffing bistability for amplification of small displacement signals in micro-devices [36] [37]. However, Duffing resonators require external forcing for sustained motion; In Section 5.2, we propose and present results for a hybrid chain of coupled van der Pol - Duffing oscillators, where the former provides the driving force. Before that, in Section 5.1, we consider a chain of Duffing resonators, which is driven externally, either at one end, or from the middle.

### 5.1 Chain of Duffing Resonators

In Subsection 2.2.2 we explored the behaviour of two coupled Duffing resonators with only one of them being forced; In this section we extend the study to a chain of Duffing resonators with one of them being forced externally. The equations of motion for the chain of (forced) Duffing resonators, with  $x$ - coupling, are

$$\ddot{x}_i + \delta \dot{x}_i + \alpha x_i + \beta x_i^3 = x_{i+1} + x_{i-1} - 2x_i, \quad i = 1, 32 \quad (i \neq l)$$

$$\ddot{x}_l + \delta \dot{x}_l + \alpha x_l + \beta x_l^3 = x_{l+1} + x_{l-1} - 2x_l + \Gamma \cos(\omega t), \quad (5.1)$$

where both ends of the chain are free ( $x_0 = x_{33} = 0$ ), and, either  $l=1$  (end forcing) or  $l=16$  (mid-forcing) in a chain of 32 resonators. For  $x$ -coupling, we first present the results for numerically solving Equation (5.1) for  $\alpha = \beta = \Gamma = 1$ , and,  $\delta = 0.1$  (Duffing A system); When the driving frequency  $\omega < 1.0$ , there is very little coupling between the resonators. For  $\omega \approx 1.0$  to  $\omega \approx 1.6$ , the amplitude of the resonators in the chain increases with frequency. Figures 5.1 and 5.2, respectively, present the time trajectories and oscillator displacements along the chain for the case of end-forcing and mid-forcing for  $\omega = 1.6$ . Partial entrainment is seen for the chain of resonators with end-forcing, whereas the chain with mid-forcing is unsynchronised. (Although the measure of synchronisation, calculated using Equation (4.3), is low for both chains,  $C_s \approx 0.005$  for the chain with mid-forcing is much smaller than that for the corresponding chain with end-forcing ( $C_s = 0.022$ ).)

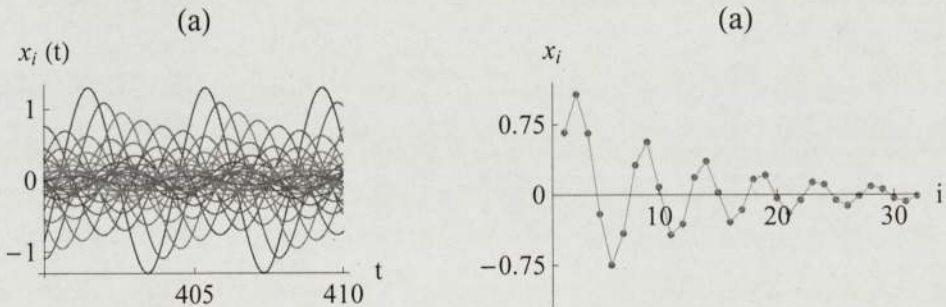


Figure 5.1: The time trajectories (a), and, oscillator displacements along the chain (b), for a chain of  $x$ - coupled Duffing resonators forced with frequency  $\omega = 1.6$  from one end.

As  $\omega$  is increased further, the displacement of the resonators away from the forcing begins to decrease, so much so that, at  $\omega = 2.2$ , the displacement for most of the chain is negligible; this is shown in Figure 5.3 for the chain with end-forcing and mid-forcing at  $t=406$ . By  $\omega = 2.5$ , the displacement of the whole chain (except for the forced resonator) is  $\approx 0$ . This is similar to the behaviour of single- and two-coupled Duffing resonators (Figure 2.7 (a) and Figure 2.11, respectively); however, no jump phenomena was seen for the chains of Duffing resonators.

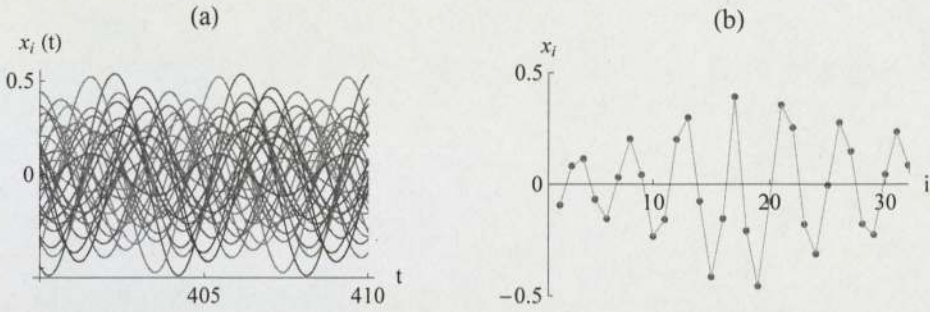


Figure 5.2: The time trajectories (a), and, oscillator displacements along the chain (b), for a chain of  $x$ - coupled Duffing resonators forced with frequency  $\omega = 1.6$  from the middle of the chain.

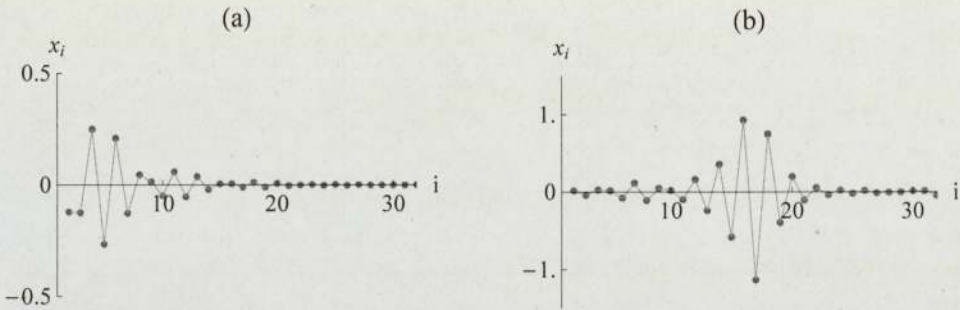


Figure 5.3: The oscillator displacements along the chain of Duffing resonators forced with frequency  $\omega = 2.3$ , from one end of the chain (a), and, from the middle of the chain (b).

We have also used equations similar to Equations (5.1) to study the cooperative behaviour of chains of velocity-coupled Duffing resonators. As can be seen from Figures 5.4 and 5.5, in contrast to the  $x$ -coupling (figures 5.1 and 5.2), the velocity-coupling is not very effective in coupling the chain of Duffing resonators; this is in contrast to the case of two coupled Duffing resonators, Section 2.2.2, where the velocity was seen to be an effective coupling mechanism.

Additionally, unlike the case of two-coupled resonators, (Subsection 2.2.2), chains of Duffing B resonators ( $\alpha = 100, \beta = 10, \delta = 0.1$  and  $\Gamma = 5$ ) were found *not* to couple with each other significantly for either  $x$ - or velocity- coupling.

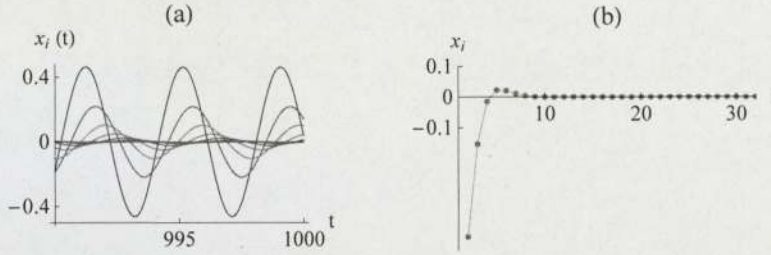


Figure 5.4: The time trajectories (a), and, oscillator displacements along the chain (b), for a velocity-coupled chain of Duffing resonators forced with frequency  $\omega = 1.6$  from one end.

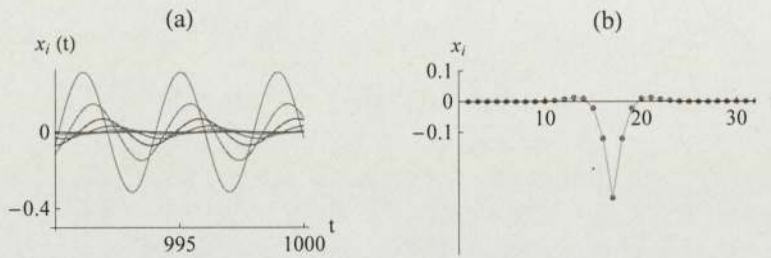


Figure 5.5: The time trajectories (a), and, oscillator displacements along the chain (b), for a velocity-coupled chain of Duffing resonators forced with frequency  $\omega = 1.6$  from from the middle of the chain.

## 5.2 Hybrid Duffing - van der Pol Systems

In this Section, we present the results of coupling van der Pol oscillator with Duffing resonators so that the former acts as driver for the latter. Two geometries have been considered:

- (i) Chain of alternating van der Pol - Duffing systems;
- (i) Chain of Duffing resonators driven by a single van der Pol oscillator at either one or both ends.

Both linear diffusive  $x$ - and velocity- couplings have been considered. Once again, we found that Duffing B resonator did not couple effectively with other Duffing resonators or with the van der Pol oscillator. Therefore, the results presented in this section are for the Duffing A system ( $\alpha = \beta = \Gamma = 1$  and  $\delta = 0.1$ ) only.

### 5.2.1 Alternating Duffing - van der Pol Oscillators

The equations of motion for the chain of oscillators/resonators are:

$$\begin{aligned} \ddot{x}_{2i+1} + \mu(x_{2i+1}^2 - 1)\dot{x}_{2i+1} + \rho x_{2i+1} &= u(x_{2i+1}) \quad i = 0, 15 \\ \ddot{x}_{2i+2} + \delta\dot{x}_{2i+2} + \alpha x_{2i+2} + \beta x_{2i+2}^3 &= u(x_{2i+2}) \quad i = 0, 15 \end{aligned} \quad (5.2)$$

where,  $u(x_i) = x_{i+1} + x_{i-1} - 2x_i$  for  $x$ - coupling and  $u(x_i) = \dot{x}_{i+1} + \dot{x}_{i-1} - 2\dot{x}_i$  for velocity coupling, with  $x_0 = \dot{x}_0 = x_{33} = \dot{x}_{33} = 0$ .

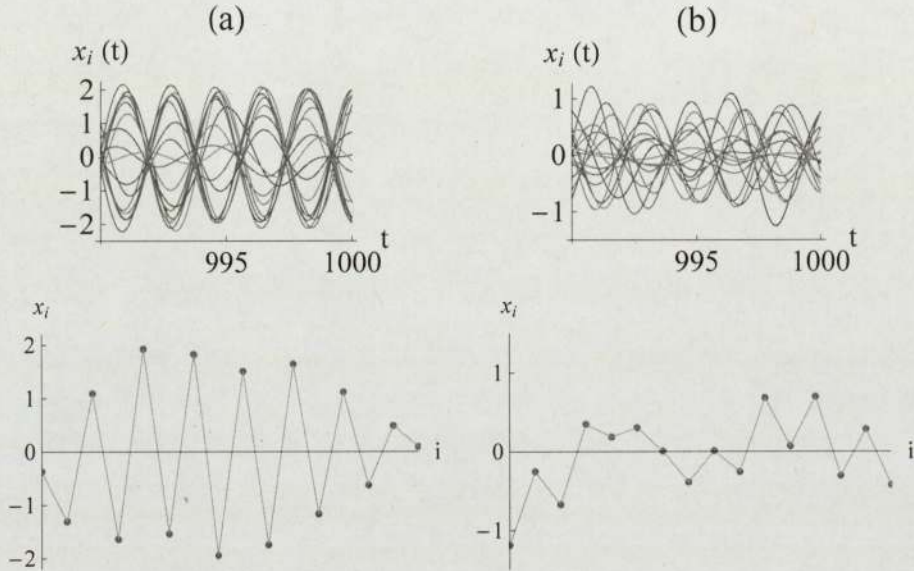


Figure 5.6: Time trajectories and displacement along the chain for (a) the van der Pol sublattice, and, (b) for the Duffing sublattice, for  $\mu = 0.1$ . Both time trajectories and oscillator displacement show that the van der Pol sublattice is more entrained compared to the Duffing sublattice.

A general result of these experiments is that the chain of alternate Duffing resonators and van der Pol oscillators evolves into two sub-lattices, each composed of oscillators of similar type. This is shown in Figure 5.6 for  $\mu = 0.1$  and  $x$ - coupling. For this case ( $\mu = 0.1$ ), the sublattice of van der Pol oscillators shows a behaviour similar to that of chain of  $x$ - coupled van der Pol oscillators (Subsection 4.2.3), where most of the van der Pol oscillators form two groups synchronised within the group and anti-phase locked with each other. The Duffing sublattice, on the other hand, is unsynchronised. The same sublattice behaviour is seen for other values of  $\mu$  as well, as

shown in Figure 5.7 for  $\mu = 1$ , where the sublattice of van der Pol oscillators is more entrained compared to the Duffing sublattice.

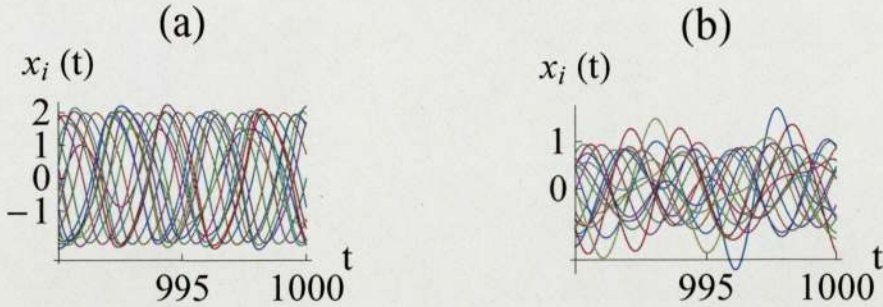


Figure 5.7: Time trajectories for (a) the van der Pol sublattice, and (b) for the Duffing sublattice, for  $\mu = 1$ .

For the case of velocity coupling and  $\mu = 0.1$ , the amplitudes of both van der Pol oscillators and Duffing resonators in the hybrid chain decay, instead of the sustained oscillations seen for the  $x$ - coupling (Figure 5.6); the rate of amplitude decay depends on  $\delta$ , the damping term for the Duffing system. For  $\mu = 1$  and velocity coupling, on the other hand, not only do we get sustained motion for both the sublattices, the van der Pol as well as the Duffing sublattice exhibit synchronisation; This is shown in Figure 5.8, where the phase portraits of 32 oscillators are seen to merge into two limit cycles, one for each sublattice.

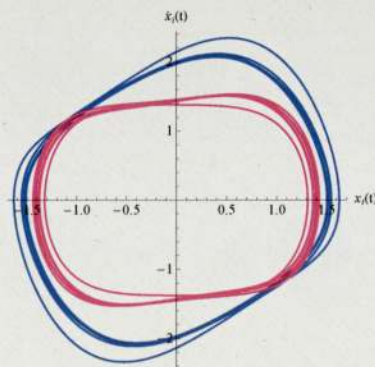


Figure 5.8: Phase portraits of velocity-coupled chain of alternating van der Pol and Duffing oscillators for  $\mu = 1$  for van der Pol sublattice (blue) and for the Duffing sublattice (magenta).

Figure 5.9 shows the time trajectories for the two sublattices, where it is seen that

the motion of oscillators in each subgroup is time-delayed with their neighbours by a constant amount, so that shifting the displacement of the oscillators along the chain by a constant time delay results in almost total synchronisation. From Figure 5.9 it is also seen that the same time delay leads to total synchronisation for both sublattices; This could also be viewed as total phase synchronisation for the whole hybrid chain of van der Pol oscillators and Duffing resonators.

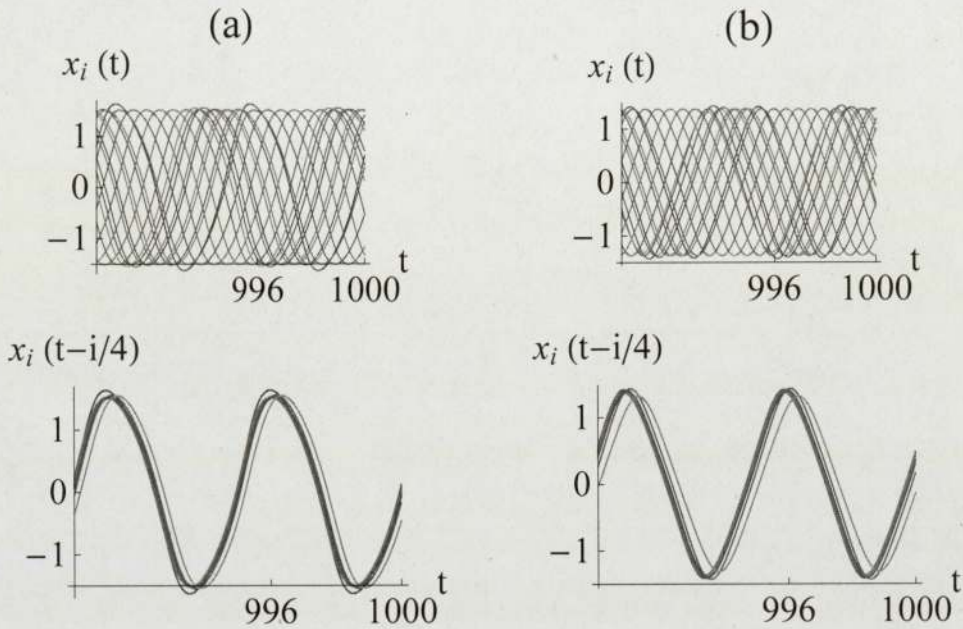


Figure 5.9: Time trajectories for the van der Pol (a) and the Duffing (b) sublattices for  $\mu = 1$ , showing time-delay synchronisation.

A similar behaviour of delay-synchronisation for both van der Pol and Duffing sublattices has been seen for a range of values of  $\mu$ , and also for other values of  $\alpha$  and  $\beta$ , with  $\mu = 1$ . As shown in Figure 5.10, the instantaneous displacement for both van der Pol and Duffing sublattices exhibits an ordered wave-like pattern, which moves to higher frequency modes with increasing  $\mu$  for  $\mu < 5$ . For  $\mu = 5$ , though the chain still forms two sublattices, the the delayed synchronisation is not there.

*The strong effect of velocity coupling seen here is in contrast with the case of velocity coupling for a chain of Duffing resonators (Section 5.1, where velocity was not found to be an effective coupling mechanism. Therefore, incorporating electrical circuits or actuators with van der Pol oscillator-like characteristics, in an array of Duffing-like*

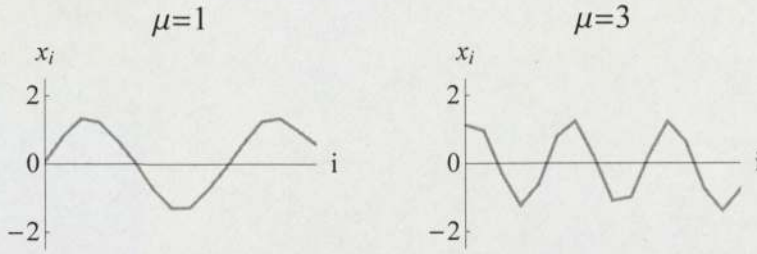


Figure 5.10: Instantaneous displacement along the chain for a velocity-coupled chain of alternating Duffing and van der Pol systems. The displacement pattern for the van der Pol and the Duffing sublattices is similar.

MEMS resonators, will result in greater coupling efficiency, especially when velocity coupling is more desirable.

### 5.2.2 Duffing Chain Driven by van der Pol Oscillators

The equations of motion for the chain of oscillators/ resonators are:

$$\begin{aligned} \ddot{x}_i + \delta \dot{x}_i + \alpha x_i + \beta x_i^3 &= u(x_i) \quad i = 2, 31 \\ \ddot{x}_j + \mu(x_j^2 - 1)\dot{x}_j + x_j &= k_j u(x_j) \quad j = 1; 32 \end{aligned} \quad (5.3)$$

where  $u(x_i)$  are as defined for Equation (5.2), and  $k_j$  is the strength for coupling between the chain of the Duffing resonators and the  $j^{\text{th}}$  van der Pol oscillator. We here consider the cases of both-ends forcing ( $k_1 = k_{32} = 1$ ), and, one-end forcing ( $k_1 = 1, k_{32} = 0$ ) for the chain of Duffing A system. Considering the case of  $x$ - coupling first, Figure 5.11 presents the time trajectories and, instantaneous displacements along the chain, for the chain of Duffing resonators coupled to van der Pol oscillators at both ends ( $\mu = 0.1$ ). From the figure, it is seen that, as in the case of chains alternating Duffing and van der Pol systems (Subsection 5.2.1), Duffing resonators form two sublattices, this time one from each half of the chain. As  $\mu$  increases, the displacement of Duffing resonators in the middle of the chain (furthest from the forcing van der Pol oscillators) decreases, so much so that, at  $\mu = 5$ , most of the chain has negligible displacement.

The formation of two sublattices, for end - forcing of Duffing chain with van der Pol oscillator, is seen more clearly for the case of *velocity coupling* for  $\mu = 0.3$  (Figs. 5.12),

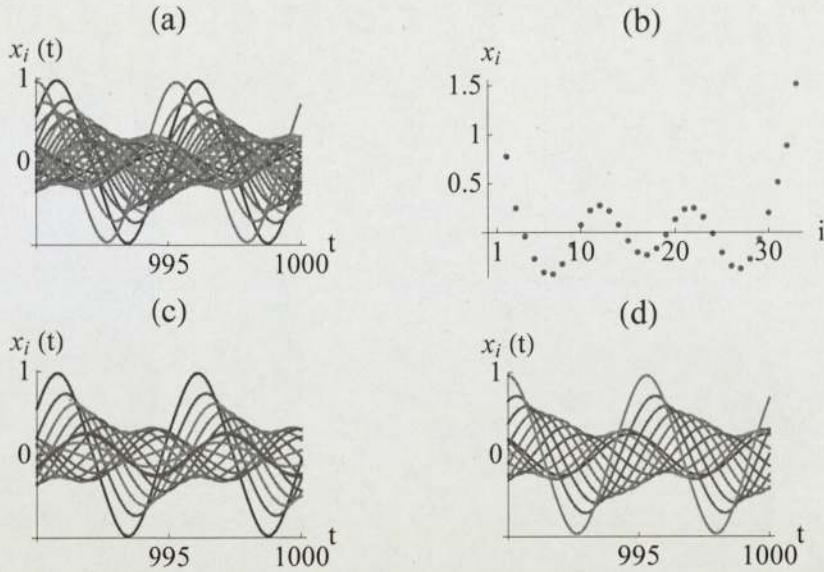


Figure 5.11: Time trajectories (a), and displacement along the chain (b), for the chain of  $x$ - coupled Duffing resonators with van der Pol forcing at both ends. The chain of Duffing resonators forms two sublattices as shown by splitting the time trajectories : (c) from  $i = 2, 16$  and (d) from  $i = 17, 31$ .

where resonators within each sublattice have almost the same phase (but different amplitudes), and the two sublattices are almost in anti-phase with each other. The relative phases of the two sublattices changes with changing  $\mu$ ; Also, as in the case of  $x$ - coupling, the displacement of the resonators in the middle of the chain decreases as  $\mu$  increases,

For the case of forcing from one end only ( $k_1 = 1, k_{32} = 0$ ), the chain of Duffing resonators behaves similar to a single sublattice in the case of forcing at both ends. The resonator displacement along the chain for  $x$ - and velocity coupling is shown in Figure 5.13, where it is seen that the resonator displacement decays along the chain. Therefore, for MEMS application purposes, in order to get significant displacement, the forcing needs to be reinforced by inserting van der Pol oscillators dispersed throughout the chain.

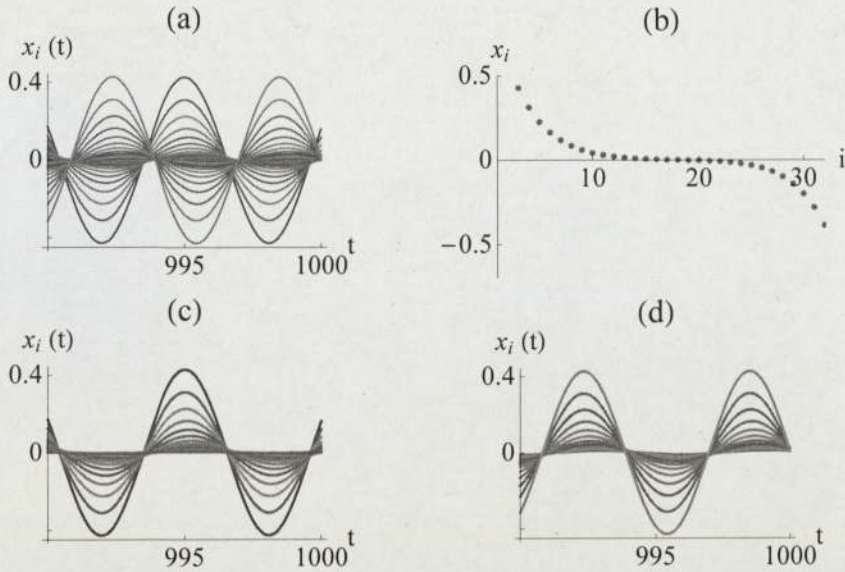


Figure 5.12: Time trajectories (a), and displacement along the chain (b), for the chain of velocity- coupled Duffing resonators with van der Pol forcing at both ends ( $i = 1, 32$ ). The chain of Duffing resonators forms two sublattices as shown by splitting the time trajectories : (c) from  $i = 2, 16$  and (d) from  $i = 17, 31$ .

### 5.3 Summary and Relevance to MEMS Arrays

In this section we summarise the results obtained in this chapter in the context of arrays of MEMS and their applications. As we have already seen in Sections 1.1 and 4.1.2, arrays of MEMS have the potential for applications in wide-ranging fields from mechanical neurocomputing to discrete transmission lines, to optical and thermal sensors. It was also seen in Sections 2.1.3 and 1.2.1 that the nonlinear properties of many of these MEMS devices can be effectively studied using the Duffing equation, and, the nonlinear properties of the Duffing resonator near resonance harnessed for various MEMS application.

In this chapter, we first studied the collective response of a linear chain of Duffing resonators which was driven either from one end or from the middle of the chain. We found that the velocity-coupling was not very efficient in transferring energy from the driven resonator to the rest of the chain, while a resonance-like behaviour was seen for the  $x$ -coupling, as the driving frequency was varied. We next studied a chain of alternating Duffing resonators and van der Pol oscillators (with no external forcing) and

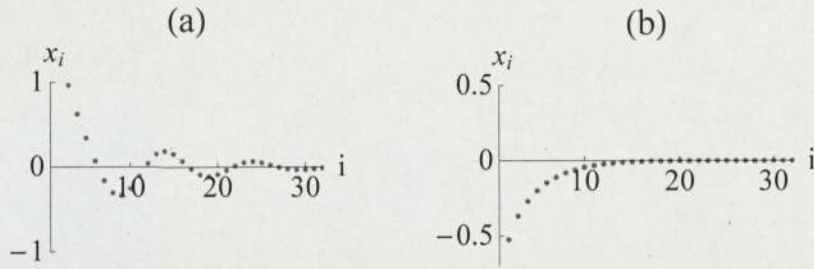


Figure 5.13: Displacement along the chain for the Duffing resonators with van der Pol forcing at one end only (a) for  $x$ -coupling, and (b) for velocity coupling.

found that both the  $x$ -coupling and the velocity coupling lead to strong displacement throughout the chain. Also, both couplings lead to the formation of sublattices, where the oscillator/ resonator of each type grouped together. For  $x$ -coupling, entrainment was seen for the van der Pol sublattice but not for the Duffing sublattice. Velocity coupling, on the other hand, resulted in phase-locked synchronisation in both sublattices for a range of parameters.

We also considered the end forcing of a chain of Duffing resonators with van der Pol oscillators. Once again, the Duffing resonators grouped into two sublattices; In this case the resonator displacement was seen to decay as the separation from the van der Pol oscillator increased.

Therefore, the performance of a chain of Duffing resonators can be substantially improved by coupling them with van der Pol oscillators, which also act as drivers for the resonators. The introduction of van der Pol oscillators in a chain of Duffing resonators is specially effective for the case of velocity coupling, which was found not to couple Duffing resonators well.

# Chapter 6

## Conclusions

In this project we have studied the synchronisation properties of diffusively-coupled nonlinear systems such as van der Pol oscillator and Duffing resonator, with a view to MEMS and NEMS applications; Both linear displacement- and velocity couplings were considered. In addition to numerical simulations, we used linear perturbation theory and the partial contraction theory to investigate the synchronisation aspects of two coupled- and one- dimensional chains of these systems; The results are summarised below:

- For velocity coupled van der Pol oscillators (both two-coupled and chains), our numerical simulations indicated asymptotic complete synchronisation for all coupling strengths,  $\kappa$ , considered. We found that our results were consistent with linear perturbation theory when the expansion was around the limit cycle (Section 4.5). Partial contraction theory, on the other hand, gives a critical value for  $\kappa$ ,  $\kappa_c$ , so that total synchronisation is predicted for all  $\kappa > \kappa_c$ . Since the results of partial contraction theory apply to the whole of the initial- value space, while our numerical simulations sample only part of it, there is no contradiction between the theory and our numerical results. Therefore, our numerical experiments suggest that, in order to obtain complete synchronisation in practical systems, it may not be necessary to have as strong a coupling as predicted by the theory.
- For the  $x$ -coupling, the two coupled van der Pol oscillators exhibit either in-phase

or anti-phase synchronisation (Subsection 2.2.1); the chains of  $x$ -coupled van der Pol oscillators, on the other hand, were seen to exhibit partial synchronisation, as evidenced by calculating the measure of synchronisation,  $C_s$  (Figure 4.9). However, as we saw in Section 4.3.2, incorporation of the cubic spring constant term resulted in complete synchronisation of the system. This system can be viewed as a Duffing resonator with nonlinear damping (and no external forcing).

- The forced Duffing resonator, with its cubic spring constant, has been used widely to study the nonlinearities in MEMS and NEMS (Section 2.1.3). We explored the nonlinear properties of a single resonator near resonance for a number of parameters, including those for real MEMS devices. This investigation was extended to the case of two-coupled and chains of Duffing resonators, where only one resonator was forced. The numerical experiments were done for two sets of parameters, one chosen randomly (Duffing A), and the other from experiments [31] (Duffing B). For the two-coupled system we found that, close to resonance, both displacement and velocity were an effective coupling mechanisms for both Duffing A and Duffing B (Subsection 2.2.2). For a chain of Duffing resonators, on the other hand, velocity was seen to be an ineffective coupling mechanism for either systems; for Duffing B system even displacement coupling was not an effective coupling mechanism (Section 5.1).
- Finally, we have proposed a hybrid chain of Duffing resonators coupled to the van der Pol oscillators. Two geometries were considered, one with alternating van der Pol - Duffing systems (Subsection 5.2.1), and two, a chain of Duffing resonators driven by a van der Pol oscillator, either from one end only, or from both ends (Subsection 5.2.2). The Duffing B system was found not to couple well with the van der Pol oscillators. On the other hand, hybrid chains of Duffing A resonator and van der Pol oscillators showed strong effects with both  $x$ - and velocity coupling. For chains of alternating Duffing A - van der Pol systems, the oscillators/ resonators grouped into two sublattice, each composed of identical oscillators. For  $x$ -coupling, the sublattice of van der Pol oscillators was more

## CHAPTER 6. CONCLUSIONS

entrained compared to the Duffing sublattice. For velocity coupling, on the other hand, delay synchronisation was seen in both sublattice for a range of oscillator parameters (Subsection 5.2.1). Thus, hybrid chains of velocity- coupled Duffing- van der Pol systems has the potential application where a synchronous behaviour in an array of MEMS resonators is desirable.

- For the case of a chain of Duffing resonators being drive by a van der Pol oscillator from one or both ends, the resonator displacement decreased as the separation from the van der Pol oscillator increased, specially for velocity coupling, Therefore, for MEMS application purposes, in order to get significant displacement, the forcing needs to be reinforced by inserting van der Pol oscillators dispersed throughout the chain.

Therefore, we propose that the performance of an array of Duffing-like MEMS resonators can be significantly improved by incorporating van der Pol oscillator- like nonlinear damping in some resonators distributed along the chain. Also, complete synchronisation in these arrays could be achieved by incorporating the nonlinear damping in all the resonators.

# Appendix A

## Derivation of van der Pol Equation

In Subsection 2.1.1 we mentioned that, for  $\mu < 0$ , the electrical circuit in Figure 2.1 represents the van der Pol [29], as may be seen below:

From Kirchoff's law,

$$L \frac{dI}{dt} + R(I)I + \frac{1}{C} \int I dt = 0, \quad (\text{A.1})$$

where,  $R(I) = -r_0 + r_2 I^2$  is the negative resistance ( $r_0, r_2 > 0$ ),  $I$  is the electric current,  $L$  is the induction and  $C$  is the capacitance in the circuit. Taking time-derivative of the Equation (A.1), we get

$$L \frac{d^2 I}{dt^2} + \left( R(I) + \frac{dR(I)}{dI} I \right) \frac{dI}{dt} + \frac{1}{C} I = 0. \quad (\text{A.2})$$

Substituting for  $R(I)$ , we get

$$L \frac{d^2 I}{dt^2} + (-r_0 + 3r_2 I^2) \frac{dI}{dt} + \frac{1}{C} I = 0. \quad (\text{A.3})$$

Defining  $\mu = r_0/L$ ,  $\rho = 1/LC$ , and changing variable from  $I$  to  $x$ , where,  $I = \sqrt{r_0/(3r_2)}x$ , we recover the van der Pol equation (2.1)

$$\ddot{x} + \mu(x^2 - 1)\dot{x} + \rho x = 0. \quad (\text{A.4})$$

# Appendix B

## A Damped van der Pol Oscillator: Contraction Properties

Let us consider a second order nonlinear system

$$\ddot{x} + \mu(x^2 + \chi)\dot{x} + \omega_0^2 x = 0, \quad (\text{B.1})$$

where,  $\mu, \chi > 0$ . This represents a damped van der Pol system, where both the time and phase trajectories go to zero. Linearising Equation (B.1), we can write

$$\begin{aligned} \dot{x} &= -\mu \frac{x^3}{3} - \mu\chi x + \omega_0 y \\ \dot{y} &= -\omega_0 x, \end{aligned} \quad (\text{B.2})$$

so that the Jacobian of the system is

$$F_{d-vdP} = \begin{pmatrix} -\mu(x^2 + \chi) & \omega_0 \\ -\omega_0 & 0 \end{pmatrix}. \quad (\text{B.3})$$

The Jacobian  $F_{d-vdP}$  is negative definite, and the system is contracting, if

$$X = [x \ y] F_{d-vdP} \begin{bmatrix} x \\ y \end{bmatrix} < 0. \quad (\text{B.4})$$

Substituting from Equation (B.3), and doing the maths, we get

$$X = -\mu(x^2 + \chi)x^2. \quad (\text{B.5})$$

From Equation (B.5) we see that X is always negative, except for when  $x=0$ ; Therefore,  $F_{d-vdP}$  is semi-negative definite, and the system is semi-contracting.

# Appendix C

## Linear Perturbation Theory for a Chain of Oscillators

In this section we shall focus on a chain of *velocity coupled van der Pol oscillators*, Equation (4.2.2)

$$\ddot{x}_i + \mu(x_i^2 - 1)\dot{x}_i + \rho x_i = \mu\kappa(\dot{x}_{i+1} + \dot{x}_{i-1} - 2\dot{x}_i) \quad i = 1, 32. \quad (\text{C.1})$$

where we consider linear perturbation around the limit cycle, so that

$$x_i(t) = x_0(t) + \xi_i(t), \quad (\text{C.2})$$

where, as discussed in Section 4.5,

$$x_0(t) = A \cos(\Omega t - \Phi), \quad (\text{C.3})$$

Where  $A = 2$ . Expanding Equation (C.1) around  $x_0$  and retaining terms linear in  $\xi$  only, we get

$$\ddot{\xi}_i + \mu[(x_0^2 - 1)\dot{\xi}_i + 2x_0\dot{x}_0\xi_i] + \rho\xi_i = \mu\kappa(\dot{\xi}_{i+1} + \dot{\xi}_{i-1} - 2\dot{\xi}_i) \quad i = 1, 32. \quad (\text{C.4})$$

From Equation (C.3) we have  $x_0^2 = 2\{1 + \cos[2(\Omega t - \Phi)]\}$  and  $x_0\dot{x}_0 = 2\sin[2(\Omega t - \Phi)]$ ; Therefore, substituting for  $x_0^2$  and  $x_0\dot{x}_0$  into Equation (C.1), and neglecting higher harmonics of  $\Omega t$ , we get

$$\ddot{\xi}_i + \mu 1 \dot{\xi}_i + \rho \xi_i = \mu \kappa (\dot{\xi}_{i+1} + \dot{\xi}_{i-1} - 2 \dot{\xi}_i) \quad i = 1, 32. \quad (\text{C.5})$$

Equation (C.5) can be rewritten as

$$\dot{\xi} = \Psi\xi, \quad (\text{C.6})$$

where,

$$\Psi = \begin{pmatrix} \bar{F}_1 - \bar{k} & \bar{k} & 0 & \cdots & 0 & 0 & 0 \\ \bar{k} & \bar{F}_2 - 2\bar{k} & \bar{k} & \cdots & 0 & 0 & 0 \\ \vdots & \vdots & \vdots & \ddots & \vdots & \vdots & \vdots \\ 0 & 0 & 0 & \cdots & \bar{k} & \bar{F}_{31} - 2\bar{k} & \bar{k} \\ 0 & 0 & 0 & \cdots & 0 & \bar{k} & \bar{F}_{32} - \bar{k} \end{pmatrix} \quad (\text{C.7})$$

with

$$\bar{F}_i = \begin{bmatrix} 0 & 1 \\ -\rho & -\mu \end{bmatrix}, \quad \text{and} \quad \bar{k} = \begin{pmatrix} 0 & 0 \\ 0 & \mu\kappa \end{pmatrix}. \quad (\text{C.8})$$

Equation (C.7) can be decomposed into  $\Psi = \bar{F} + \bar{K}$ , where,

$$\bar{F} = \begin{pmatrix} \bar{F}_1 & 0 & \cdots & 0 & 0 \\ 0 & \bar{F}_2 & \cdots & 0 & 0 \\ \vdots & \vdots & \ddots & \vdots & \vdots \\ 0 & 0 & \cdots & \bar{F}_{31} & 0 \\ 0 & 0 & \cdots & 0 & \bar{F}_{32} \end{pmatrix} \quad \text{and} \quad \bar{K} = \begin{pmatrix} -\bar{k} & \bar{k} & 0 & \cdots & 0 & 0 & 0 \\ \bar{k} & -2\bar{k} & \bar{k} & \cdots & 0 & 0 & 0 \\ \vdots & \vdots & \vdots & \ddots & \vdots & \vdots & \vdots \\ 0 & 0 & 0 & \cdots & \bar{k} & -2\bar{k} & \bar{k} \\ 0 & 0 & 0 & \cdots & 0 & \bar{k} & -\bar{k} \end{pmatrix}. \quad (\text{C.9})$$

For  $\mu > 0$ ,  $\bar{F}_i$  is negative definite since the real part of its eigenvalues,  $\lambda_{1,2} = -\frac{\mu}{2} \pm \frac{\sqrt{\mu^2 - 4\rho}}{2}$ , is negative; Therefore,  $\bar{F}$  is also negative definite. It can also be shown, using mathematica, that the eigenvalues of  $\bar{K}$  are either zero or negative for  $\kappa > 0$ . Therefore, the Jacobian obtained for linear perturbation about the limit cycle,  $\Psi$ , is negative definite, and the system of *velocity* - coupled chain of van der Pol oscillators synchronises asymptotically for coupling constant  $\kappa > 0$ .

# Bibliography

- [1] W. Wang and J. J. E. Slotine. On partial contraction analysis for coupled nonlinear oscillators. *Biological Cybernetics*, 92:38–53, 2005.
- [2] R. M. C. Mestrom, R. H. B. Fey, I. T. M. van Beek, K. L. Phan, and N. Nijmeijer. Modelling the dynamics of a MEMS resonator: Simulations and experiments. *Sensors and Actuators A*, 142:306–315, 2008.
- [3] R. M. C. Mestrom, R. H. B. Fey, and N. Nijmeijer. On phase feedback for nonlinear MEMS resonators. In *Proceedings of the IEEE Frequency Control Symposium*, Geneva, Switzerland, May 2007.
- [4] H. W. Ch Postma, I. Kozinsky, A. Husain, and M. L. Roukes. Dynamic range of nanotube- and nanowire-based electromechanical system. *Applied Physics Letters*, 86:223105, 2005.
- [5] Y. Huang and Y. Tamum. Investigation of the stability of the power system governed by Duffing's equation. In *IEEE TENCON*, Beijing, China, 1993.
- [6] A. Pikovsky, M. Rosenblum, and J. Kurths. *Synchronization: A Universal Concept in Non-Linear Sciences*. Cambridge University Press, 2001.
- [7] H. B. Fostin and P. Woaf. Dynamics and synchronization in an electrical circuit consisting of a van der Pol oscillator coupled to a Duffing oscillator. *Physica Scripta*, 71:141–147, 2005.
- [8] N. Maluf and K. Williams. *An Introduction to Microelectromechanical Systems Engineering*. Artech House Inc., 2004.

## BIBLIOGRAPHY

- [9] S. Beeby, G. Ensell, M. Kraft, and N. White. *MEMS: Mechanical Sensors*. Artech House Inc, 2004.
- [10] Z. E. Wang, W. Cao, X. C. Shan, J. F. Xu, S. P. Lim, W. Noell, and N. F. de Rooij. Development of  $1 \times 4$  MEMS-based optical switch. *Sensors and Actuators A*, 114:80–87, 2004.
- [11] E. Buks and M. L. Roukes. Electrically tunable collective response in a coupled micromechanical array. *Journal of Micromechanical Systems*, 10:802–807, 2002.
- [12] F. C. Hoppensteadt and E. U. Izhikevich. Synchronization of mems resonators and mechanical neurocomputing. *IEEE Transactions on Circuits and Systems-I: Fundamental Theory and Applications*, 48:133–138, 2001.
- [13] R. M. Lin and W. J. Wang. Structural dynamics of microsystems - current state of research and future directions. *Mechanical Systems and Signal Processing*, 20:1015–1043, 2006.
- [14] V. Kaajakari, T. Mattila, A. Lipsanen, and A. Oja. Nonlinear mechanical effects in silicon longitudinal mode beam resonators. *Sensors and Actuators A*, 120:64–70, 2005.
- [15] V. Kaajakari. Electrical equivalent circuits for microprocessors. Website <http://www.kaajakari.net> links to MEMS tutorials.
- [16] A. Cavagna, I. Giardina, A. Orlandi, G. Parisi, A. Procaccini, M. Viale, and V. Zdravkovic. The STARFLAG handbook on collective animal behaviour: Part I, empirical methods. *Quantitative Biology: Quantitative Methods*, 2008.
- [17] S. H. Strogatz. From Kuramoto to Crawford: Exploring the onset of synchronization in populations of coupled oscillators. *Physica D*, 143:1–20, 2000.
- [18] A. M dos Santos, S. R. Lopes, and R. L. Viana. Rhythm synchronization and chaotic modulation of coupled van der Pol oscillators in a model for the heartbeat. *Physica A*, 338:335–355, 2004.

## BIBLIOGRAPHY

- [19] M. Lees, B. Logan, and G. Theodoropoulos. Adaptive optimistic synchronisation for multi-agent distributed simulation. In D. Al-Dabass, editor, *Proceedings of the Seventeenth European Simulation Multiconference*, pages 77–82. Society for Modelling and Simulation International, 2003.
- [20] S. N. Dorogovtsev and J. F. F. Mendes. *Evolution of Networks*. Oxford University Press, 2003.
- [21] W. O. Criminale, T. L. Jackson, and P. W. Nelson. Limit cycle strange attractor competition. *Studies in Applied Mathematics*, 112:133–160, 2004.
- [22] H. G. Enjieu Kadji and R. Yamapi. General synchronization dynamics of coupled van der Pol-Duffing oscillations. *Physica A*, 370:316–328, 2006.
- [23] S. P. Raj, S. Rajasekar, and K. Murali. Coexisting chaotic attractors, their basin of attraction and synchronization of chaos in two coupled Duffing oscillators. *Physica Letters A*, 264:283–288, 1999.
- [24] B. K. Shivamoggi. *Perturbation Methods for Differential Equations*. Birkhäuser, Boston, 2nd edition, 2003.
- [25] D. W. Jordan and P. Smith. *Nonlinear Ordinary Differential Equations*. Clarendon Press, Oxford, second edition, 1987.
- [26] X. Xiong, J. Wang, and T. Zhou. Contraction principal and its application in synchronization in nonlinearly coupled systems. *Chaos, Solitons and Fractals*, 32:1147–1153, 2007.
- [27] van der Pol oscillator. Wikipedia, the free encyclopedia- <http://en.wikipedia.org>.
- [28] B. van der Pol and J. van der Mark. Frequency demultiplication. *Nature*, 120:363–364, 1927.
- [29] S. Nagano. Biological receptor scheme for the robust synchnization of limit cycle oscillators. *Progress in Theoretical Physics*, 107:861–877, 2002.

## BIBLIOGRAPHY

- [30] M. Lakshmanan and K. Murali. *Chaos in Nonlinear Oscillators: Controlling and Synchronization*. World Scientific, 1996.
- [31] C. Deng and S. Collins. Duffing resonators. Seminar presentation, April 2008.
- [32] E. Buks and B. Yurke. Mass detection with nonlinear nanomechanical resonator. *Physical Review E*, 74:046619, 2006.
- [33] O. Kogan. Controlling transitions in a Duffing oscillator by sweeping parameters in time. *Physical Review E*, 76:037203, 2007.
- [34] W. Zhang, R. Baskaran, and K. L. Turner. Effect of cubic nonlinearity on auto-parametrically amplified resonant MEMS mass sensor. *Sensors and Actuators A*, 102:139–150, 2002.
- [35] A. A. Batista, F. A. Oliveira, and N. H. Nazareno. Duffing resonator: Control and memory effects. *Physical Review E*, 77:066216, 2008.
- [36] R. Almog, S. Zaitsev, O. Stempluck, and E. Buks. High intermodulation gain in a micromechanical Duffing resonator. *Applied Physics Letters*, 88:213509, 2006.
- [37] R. Almog, S. Zaitsev, O. Stempluck, and E. Buks. Noise squeezing in a micromechanical Duffing resonator. *Physical Review Letters*, 98:078103, 2007.
- [38] L. Grasser, H. Mathias, F. Parrain, X. L. Roux, and J.-P. Gilles. MEMS Q-factor enhancement using parametric amplification: Theoretical study and design of a parametric device. In *DTIP of MEMS and MOEMS*, Stresa, Italy, 2007.
- [39] P. S. Addison. On the characterization of the nonlinear oscillator systems in chaotic mode. *Journal of Sound and Vibration*, 179:385–398, 1995.
- [40] M. C. Cross, A. Zumdieck, R. Lifshitz, and I. L. Rogers. Synchronization by nonlinear frequency pulling. *Physical Review Letters*, 93:224101, 2004.
- [41] L. A. Low, P. G. Reinhall, and D. W. Storti. An investigation of coupled van der pol oscillators. *Transactions of the ASME*, 125:162–169, 2003.

## BIBLIOGRAPHY

- [42] D. W. Storti and R. H. Rand. Dynamics of two strongly coupled van der Pol oscillators. *International Journal of Nonlinear Mathematics*, 17:143–152, 1982.
- [43] W. Lohmiller and J. J. E. Slotine. On contraction analysis for non-linear oscillators. *Automatica*, 34:683–696, 1998.
- [44] J.-S. Fang, Z. Fang, X. J. Liu, and M.-S. Rong. Chaos synchronization in two-coupled Duffing oscillators. *Chinese Physica Letters*, 18:1438–1441, 2001.
- [45] Q-C Pham and J. J. E. Slotine. Stable concurrent synchronization in dynamic system networks. *Neural Networks*, 20:62–77, 2007.
- [46] T. Dauxois, M. Peyrard, and S. Ruffo. The Fermi-Pasta-Ulam ‘numerical experiment’: History and pedagogical perspectives. *European Journal of Physics*, 26:S3–S11, 2005.
- [47] K. Yushimora and Y. Doi. Moving discrete breathers in non-linear lattice: Resonance and stability. *Wave Motion*, 45:83–99, 2007.
- [48] A. J. Lichtenberg and V. V. Mirnov. Stability of an oscillator chain from high-frequency initial conditions. *Physics D*, 202:116–133, 2005.
- [49] E. Fermi, J. Pasta, and S. Ulam. Technical report, 1955.
- [50] V. Koukouloyannis I. Koukaris. Existence of multiple intrinsic localized modes in one-dimensional Debye crystals. *Physical Review E*, 76:016402, 2007.
- [51] R. Palamakumbura, S. Maithripala, W. P. Dayawansa, and H. Inaha. Control of traveling pulses in MEMS: Numerical evidence of practical total stabilisation. In *2005 American Control Conference*, Portland, OR, USA, 2005.
- [52] M. Sato, S. Yasui, M. Kimura, T. Hikihara, and A. J. Sievers. Management of localized energy in discrete nonlinear transmission lines. *Europhysics Letters*, 80:30002, 2007.

## BIBLIOGRAPHY

- [53] M. Sato, B. E. Hubbard, and A. J. Sievers. Colloquium: Nonlinear energy localization and its manipulation in micromechanical oscillator arrays. *Reviews of Modern Physics*, 78:137–157, 2006.
- [54] L. Kocarev and U. Paritz. Generalized synchronization, predictability, and equivalence of unidirectionally coupled dynamical systems. *Physical Review Letters*, 76:1816–1819, 1996.
- [55] GC Zuang, J. Wang, Y. Shi, and W. Wang. Phase synchronization and its cluster feature in two-dimensional coupled map lattices. *Physical Review E*, 66:146201, 2002.
- [56] T. E. Vadivasova, G. I. Strelkova, and V. S. Anishchenko. Phase-frequency synchronization in a chain of periodic oscillators in the presence of noise and harmonic forcing. *Physical Review E*, 63:036225, 2001.
- [57] P. Taas, M. G. Rosenblum, J. Weule, J. Kurthis, A. Pikovsky, J. Volkmann, A. Schmiltzer, and H.-J. Freund. Detection of the  $n:m$  phase locking from noisy data: Application to magnetoencephalography. *Physical Review Letters*, 81:3291–3294, 1998.
- [58] J. M. Hurtado, L. L. Rubchinsky, and K. A. Sigvardt. Statistical method for detection of phase-locking episodes in neural oscillations. *Journal of Neurophysiology*, 91:1883–1898, 2004.
- [59] T. Kruez, F. Mormann, R. G. Andrzejac, A. Kraskov, K. Lehnertz, and P. Grassberger. Measuring synchronization in coupled model systems: A comparison of different approaches. *Physica D*, 225:29–42, 2007.
- [60] R. Q. Quiroga, A. Krakov, T. Kruez, and P. Grassberger. Performance of different synchronization measures in real data: A case study on electroencephalographic signals. *Physical Review E*, 65:041903, 2002.

## BIBLIOGRAPHY

- [61] E. Ulnar, R. Vicente, G. Pipa, and J. G.-Ojalvo. Contour integration and synchronization in neuronal networks of the visual cortex. In *18th International Conference on Artificial Neural Networks*, Prague, Czech Republic, September 2008.
- [62] G. V. Osipov and M. M. Sushchik. The effect of natural frequency distribution on cluster synchronisation in oscillator arrays. *IEEE Transactions in Circuits and Systems-I: Fundamental Theory and Applications*, 44:1006–1010, 1997.
- [63] Wei Wang. PhD thesis.
- [64] H. G. Enjieu Kadji, J. B. Chabi Orou, and P. Wofo. Synchronization dynamics in a ring of four mutually coupled biological systems. *Communications in Nonlinear Science and Numerical Simulation*, 13:1361–1372, 2008.